Crashworthiness Assessment of the Flying-V Under Complex Crash Scenarios With Partially Detailed Structures

Ferreira da Costa, T.; Villa, Andrea; Rans, C.D.; Castro, Saullo G.P.

DOI
10.2514/6.2025-0622

Publication date
2025

Document Version
Final published version

Published in
Proceedings of the AIAA SCITECH 2025 Forum

AIAA SciTech Forum
6-10 January 2025, Orlando, FL
AIAA SCITECH 2025 Forum

10.2514/6.2025-0622

Crashworthiness Assessment of the Flying-V Under Complex Crash Scenarios with Partially Detailed Structures

T.F. da Costa, A. Villa, C. Rans, S.G.P. Castro*
Department of Aerospace Structures & Materials, Delft University of Technology, Kluyverweg Street No. 1, 2629HS, Delft, The Netherlands

Traditional aircraft crashworthiness assessments typically involve vertical drop tests on a specific fuselage segment to simulate landing impacts. However, the Flying-V's unique geometry and mass distribution challenge the suitability of such simplified tests. Previous studies have focused solely on the wing-fuselage region, neglecting the central and outboard areas. This research aims to develop a methodology for a more elaborated crashworthiness assessment, particularly for unconventional aircraft such as the Flying-V. It proposes simplified modelling approaches to capture essential kinematics without detailing the entire aircraft. A newly introduced reduced modelling technique, leveraging moments of inertia, optimizes vertical drop tests and reduces simulation time. However, limitations arise when evaluating more intricate crash scenarios, prompting the proposal of a submodelling technique. While the submodelling technique effectively captures the engine section dynamics, comprehensive finite element modelling remains essential for addressing complex scenarios.

I. Nomenclature

$a(t)$	=	resultant acceleration (measured in G) at the center of gravity of the head
G_x, G_y	=	magnitudes of acceleration along the x and y axes, respectively
g	=	earth gravitational acceleration
G_{xL},G_{yL}	=	limit value for the x and y axes, respectively
H	=	angular momentum
I_{ij}	=	moments of inertia about a generic axis
k	=	spring stiffness constant
m	=	point mass
$\mathbf{R}$	=	rotation matrix
t_1, t_2	=	initial and final times at which the HIC (head injury criteria) reaches its maximum value
T	=	kinetic energy
U	=	potential energy
z	=	acceleration input
δ	=	degree of freedom
ζ	=	damping ratio
ω_n	=	natural frequency
ω	=	angular velocity
v	=	velocity

II. Introduction

Aircraft crashworthiness has been a longstanding concern in aviation since the early days of air travel. Nowadays, the focus on crashworthiness extends to innovative aircraft configurations such as the Flying V, which features a unique V-shaped fuselage. While this design offers fuel efficiency and aerodynamic benefits, it presents unique challenges for structural design, manufacturing, and passenger safety. Traditional crashworthiness assessments, typically involving vertical drop tests on specific fuselage segments, may not be applicable due to the Flying-V's unconventional geometry and mass distribution.

*Corresponding author: S.G.P.Castro@tudelft.nl

Previous research has detailed the wing-fuselage region of the Flying-V [1–3], where most passengers and payload are located, but information on the central and outboard regions is lacking. Despite existing mass estimates for these uncovered areas [4], further investigation on the crashworthiness of the Flying-V considering this information is needed.

The primary goal of this research is to develop a methodology for assessing more comprehensive crash scenarios for unconventional aircraft like the Flying-V, where a preliminary assessment is deemed crucial even without having all the information about the structural design. We propose simplified modeling approaches that capture the essential kinematics of various sections without requiring a detailed physical representation of the entire aircraft, while keeping the focus only on the regions of interest.

III. Background

Before delving into the specifics of the work conducted, it's crucial to establish a solid foundation by understanding the key concepts that underpin this field of study.

A. Basic Principles of Crashworthiness

Crashworthiness refers to an aircraft's ability to protect its occupants from harm during and after a controlled crash by effectively utilizing its internal systems and components. It encompasses several key criteria aimed at ensuring occupant safety:

1) **Guarantee of a survivable volume:** The aircraft structure must maintain a space that can protect occupants from direct impact and intrusion during a crash;
2) **Guarantee of acceptable acceleration and loads:** The forces experienced by occupants during a crash should be within survivable limits to prevent serious injuries;
3) **Retention of items of mass:** All heavy items, such as engines and luggage, must be securely fastened to prevent them from becoming projectiles within the cabin;
4) **Preservation of occupants' egress paths**: It is crucial to maintain clear and accessible exit routes for occupants to evacuate the aircraft quickly after a crash [5].

Over the past decades, ensuring the safety of aircraft occupants during crashes has been a major concern. Significant advancements in safety measures have reduced the proportion of accidents leading to fatalities to below 50% in the past twenty years. However, a notable 46% of accidents occur during the approach and landing phases [6], underscoring the importance of robust occupant protection.

Most existing safety data pertains to conventional aircraft designs, leaving a gap in understanding novel configurations such as the Flying-V, the focus of this study. Nonetheless, meeting the stringent criteria for occupant protection is essential for advancing aviation safety in this newly design.

B. The Flying-V Aircraft Configuration

The Flying-V, depicted in Figure 1, is an innovative aircraft featuring a unique V-shaped configuration that seamlessly integrates the passenger cabin and cargo space into the main lifting surface, potentially reducing fuel consumption by up to 20% compared to an Airbus A350 for the same flight [7]. Additionally, unlike other blended-wing body concepts, the FV fuselage can be adjusted in length to create a family of aircraft variants.

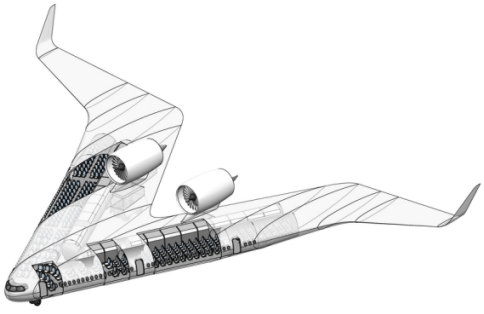

Fig. 1 Flying-V 3D geometry resulting from the conceptual study [8].

However, this design differs significantly from conventional cylindrical fuselage and wing aircraft. As illustrated in Figure 2, the oval fuselage of the Flying-V has considerably reduced crumple zone underneath the passenger floor structures $L_2 < L_1$ when compared to a conventional aircraft of similar mission, such as the Airbus A350. A large crumple zone allows more space for structural components to plastically deform and absorb more the impact forces during a controlled crash.

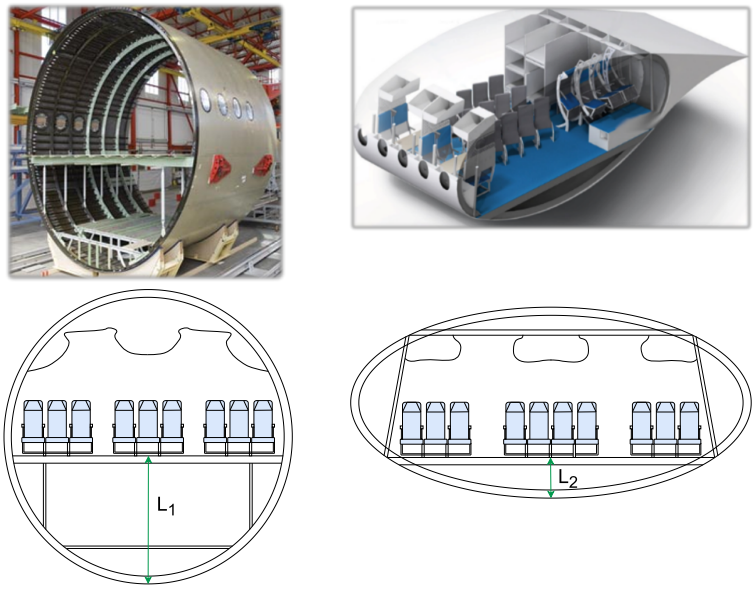

Fig. 2 Differences in crushing distance from conventional and the Flying-V aircraft design, modified from Anand et al. [9, 10].

C. Current Requirements from Regulatory Agencies

Certifying new aircraft configurations requires demonstrating that safety standards are at least comparable to those of traditional transport aircraft. Both Blended-Wing Body and Flying-V configurations must show adequate crashworthiness, particularly for emergency landings, to meet these stringent safety requirements. Regulatory agencies, such as the European Union Aviation Safety Agency (EASA) and the Federal Aviation Administration (FAA), have introduced a series of crashworthiness standards specifically for transport category airplanes [11, 12]. These standards are designed to ensure occupant safety during crash scenarios by setting rigorous criteria for various aspects of aircraft design and performance.

One key regulation is the CS-25.561 [12], which specifies the ultimate accelerations that occupants should encounter in a configuration where the landing gear is retracted:

- Upward: 3.0g;
- Forward: 9.0g;
- Sideward: 3.0g on the airframe and 4.0g on the seat and their attachments;
- Downward: 9.0g;
- Backward: 1.5g;

with these load factors being increased by 33% for any structures that must be frequently removed. These loads must be applied in static analyses to ensure that both the airframe and the seating installations can withstand significant forces during an emergency landing or crash, thereby protecting the occupants.

Additionally, CS-25.562 [12] mandates two dynamic tests under conditions depicted in Figure 3 of the regulation. These tests evaluate the performance of an aircraft seat, its restraints, and the associated interior systems under simulated crash conditions.

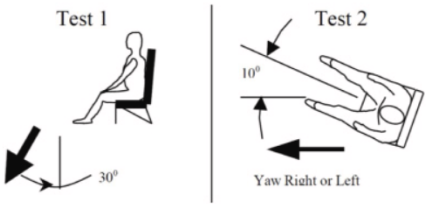

(a) CFR 25.562 Test I and Test II setup

	Test I	Test II
Min $V_1(m/s)$	10.67	13.41
Max t (s)	0.08	0.09
Min G	14	16
Roll (deg)	0	10
Pitch (deg)	0	10

(b) Test I and Test II conditions

Fig. 3 CFR 25.562 test setups and conditions [5].

However, the regulatory framework established by these agencies primarily focuses on the safety of seat installations. As a result, there is currently no comprehensive standard specifically addressing the crashworthiness of the entire aircraft structure. This omission stems from the assumption that the aircraft structure itself inherently provides an acceptable level of crashworthiness [13].

Following the dynamic conditions discussed, a set of performance criteria must be met to ensure occupant safety. One key measure is the Head Injury Criterion (HIC), which comes into play when contact between an occupant's head and the surrounding structure could occur, and can be calculated by:

$$HIC = \left\{ (t_2 - t_1) \left[\frac{1}{(t_2 - t_1)} \int_{t_1}^{t_2} a(t)dt \right]^{2.5} \right\}_{\max} \tag{1}$$

where t_1 and t_2 represent the initial and final times at which the HIC reaches its maximum value; while $a(t)$ denotes the resultant acceleration (measured in G) at the center of gravity of the head [14]. The regulations require sufficient protection such that the head impact does not exceed a HIC of 1000 points. The main drawback of calculating the HIC during preliminary design is the necessity of detailed information regarding the compliance of the interior structures within the head trajectory.

Another injury criterion relates to the lumbar loads, specifying that the maximum allowable compressive load between the pelvis and the lumbar column should not exceed 1500 pounds (680 kilograms) [15]. A significant issue with calculating the lumbar load is the need to incorporate both a seat model and an anthropomorphic dummy model to obtain meaningful results.

Desiderio et al. [2, 3] proposed the adoption of the dynamic response index (DRI) as a criterion more compatible with the preliminary design of unconventional aircraft [16]. The DRI is a well-established crash injury metric developed by the U.S. Air Force (USAF), consisting of a mathematical model designed to predict the probability of spinal injuries in pilots subjected to high-amplitude and short-duration accelerations in the +Gz direction, typically induced by ejection seats [17].

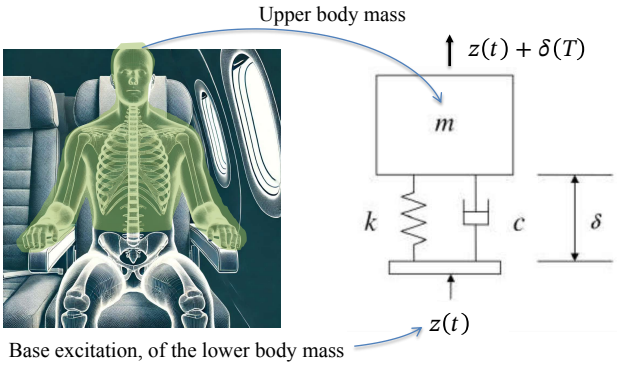

Fig. 4 Dynamic response index model.

D. Proposed Crashworthiness Requirements for the Flying-V

The following presents a detailed description of the DRI model, illustrated in Figure 4, which represents the relative displacement $\delta(t)$ between the lower and upper body mass caused by an imposed base acceleration $\ddot{z}(t)$ that acts on the

lower body mass. The equation of motion for the upper body mass m is:

$$-\delta k - \dot{\delta} c = m\ddot{z}(t) + m\ddot{\delta}(t)$$

where m is the body mass above the lumbar region (upper body); δ is the relative displacement of the upper body with respect to the lower body; k is the stiffness of the lumbar region; and c is the damping of the lumbar region. Rearranging and mass-normalizing yields:

$$\ddot{\delta}(t) + \dot{\delta}(t)\frac{c}{m} + \delta(t)\frac{k}{m} = -\ddot{z}(t)$$

and substituting with the definition of undamped natural frequency $\omega_n = \sqrt{k/m}$; and damping ratio $\zeta = c/(2\sqrt{mk})$:

$$\ddot{\delta}(t) + 2\zeta\omega_n\dot{\delta}(t) + \omega_n^2\delta(t) = -\ddot{z}(t) \tag{2}$$

Equation 2 was first presented by Coltman et al. [16], and can be solved for a general case of imposed accelerations by assuming a series of acceleration impulses p_n, each consisting of a discrete level of acceleration a_n that happens at time t_n and acts during a finite interval Δt, such that $p_n = a_n \Delta t$. Thus, the solution for each acceleration impulse becomes:

$$\delta(t) = \begin{cases} 0 & t < t_n \\ p_n h\,(t - t_n) & t \geq t_n \end{cases} \tag{3}$$

with:

$$h\,(t - t_n) = \frac{1}{\omega_d} e^{-\zeta\,\omega_n (t - t_n)} \sin \omega_d\,(t - t_n)\, H\,(t - t_n)$$

where $H(t - t_n)$ is a heavy side function; and $\omega_d = \omega_n\sqrt{1 - \zeta^2}$. Note that the solution for a given interval of interest $t_1 \leq t \leq t_2$ must consider all acceleration impulses that happened during this interval. The calculation of the DRI is:

$$\text{DRI} = \frac{\omega_n^2 \delta_{max}}{g}$$

where $g = 9.81$ m/s^2 and δ_{max} is the maximum absolute value for $\delta(t)$ in the interval $t_1 \leq t \leq t_2$. Stech and Payne [18] made a research with the U.S. Air Force (USAF) pilots, and concluded that the damping for this lumbar model is $\zeta = 0.224$, and the undamped natural frequency is $\omega_n = 52.9$ rad/s, for the 50th percentile of USAF pilots at the time. Although the DRI is generally correlated with the probability of spinal injury, its accuracy is disputable due to its derivation from decades-old data that lacked diversification in terms of age, gender, and body type. Nonetheless, it serves as a good baseline for comparison. Brinkley & Shaffer [17] presented the rate of spinal injury as a function of the DRI, as illustrated in Figure 5.

Currently, there are no explicit requirements in CS-25 or 14 CFR Part 25 regarding spinal injury following a crash landing. However, in 2018, the Transport Aircraft Crashworthiness and Ditching Working Group (TACDWG) — a commission formed by the FAA's Aviation Rulemaking Advisory Committee (ARAC) [19] to recommend new airframe-level crashworthiness and ditching standards — recognized the following [20]:

- A DRI of 16 units is an acceptable limit for crashworthiness certification, corresponding to a spinal injury rate of 3%, as depicted in Figure 5. This value corresponds to accepted values by regulatory agencies in previously certified aircraft;
- The vertical impact velocity requirement should be determined according to the aircraft's maximum take-off weight (MTOW), as illustrated in Figure 6.

Since the focus of this assessment will be given to different sections of the Flying-V, it will need to be designed according to the most stringent requirement. The MTOW of the heaviest FV variant is estimated to be 278,000 kg (613,000 lbs) [4], corresponding to a vertical impact speed of 7.9248 m/s (26 ft/sec).

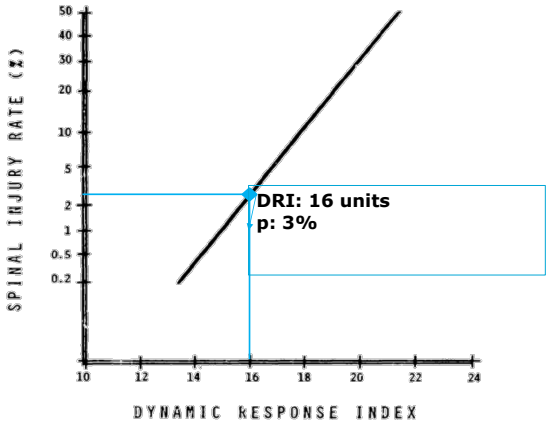

Fig. 5 Probability of spinal injury as a function of the DRI, modified from [17].

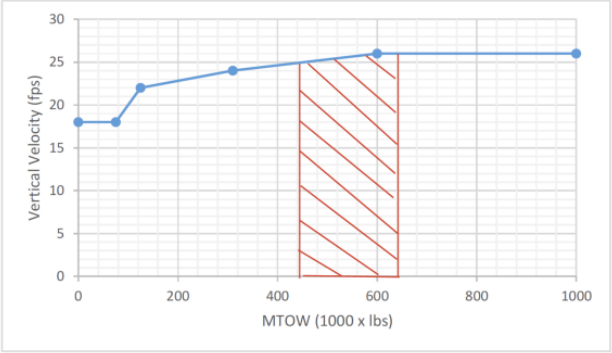

Fig. 6 Vertical impact velocity requirement vs. MTOW, adapted from TACDWG [20]. The hatched pattern by Desiderio [2] highlights the estimated MTOW range for the Flying-V family, as determined by Oosterom [4].

However, previous studies only focused on vertical drop tests, raising the question: Are vertical drop tests and the dynamic response index sufficient to assess the crashworthiness of the Flying-V? The unique design of the FV, where the constant cross-section of the wings' fuselage creates a specific angle with the landing direction, can lead to alternative passenger seat orientations not accounted for in vertical drop tests.

Vertical drop tests also fail to capture the complexity and dynamics of realistic landing scenarios, which involve horizontal, rotational, and vertical components. These tests do not fully evaluate passenger injuries in more complex landing scenarios.

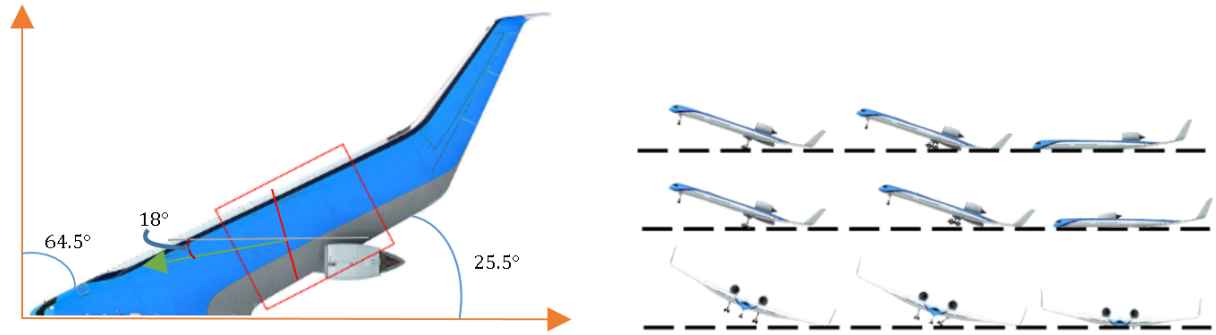

(a) Possible passenger seats orientation **(b) Possible crash sequences for the Flying-V**

Fig. 7 Unique challenges faced by the Flying-V.

While the DRI provides a good estimate of potential damage in the z-direction, making it suitable for vertical drop tests, it does not account for injuries in other possible directions. Additionally, the human body's resistance to sudden acceleration varies across different directions.

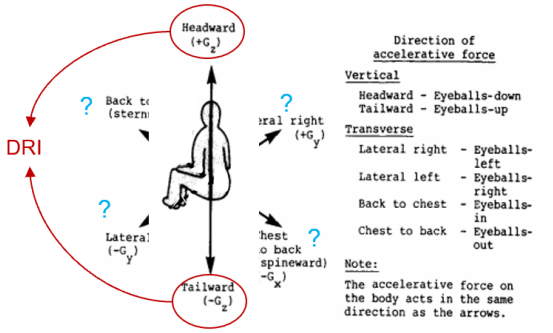

(a) Limitations of the DRI

Direction of Accelerative Force	Occupant's Inertial Response	Tolerance Level
Headward (+Gz)	Eyeballs Down	$20-25$G
Tailward (-Gz)	Eyeballs Up	15G
Lateral Right (+Gy)	Eyeballs Left	20G
Lateral Left (-Gy)	Eyeballs Right	20G
Back to Chest (+Gx)	Eyeballs Out	45G
Chest to Back (−Gx)	Eyeballs In	45G

(b) Human tolerance limits

Fig. 8 Some of the limitations posed by the DRI.

To address accelerations other than the vertical, the USAF has implemented a system that combines acceleration components and the DRI to determine acceptable acceleration environments for ejection seats. This system is outlined in Specification MIL-S-9479 [21], which regulates the levels of acceleration experienced by the occupant. Given the complexity of injury assessment, this more sophisticated criterion, known as the Severity Index (SEV), will be employed in subsequent analyses.

The SEV is determined by the following expression:

$$SEV = \left(\frac{\text{DRI}}{\text{DRI}_L}\right)^2 + \left(\frac{G_x}{G_{xL}}\right)^2 + \left(\frac{G_y}{G_{yL}}\right)^2 \tag{4}$$

where G_x and G_y represent the magnitudes of acceleration along the x and y axes, respectively, derived using the methodology explained in the Appendix. This technique determines the acceleration time history for each axis. G_{xL} is the limit value for the x axis (fore and aft) from Figures 39, 40, and 41, and G_{yL} is the limit value for the y axis (sideways) from Figure 42, also in Appendix. The DRI is the dynamic response index value computed for the positive z direction, with its limit value set to 16 units. The calculated value for the SEV should not exceed one; otherwise, passengers will sustain injuries. This will be the final injury criterion used to assess the crashworthiness of the Flying-V.

As a final note, the current objective is not to optimize the design to minimize injury criteria but to explore how various modeling approaches and crash scenarios influence spatial injury patterns among passengers. Accordingly, a SEV above one will be considered hazardous, with greater danger associated with higher values. Conversely, values below one for SEV will be deemed safe. Subsequently, the introduction of roll angles and pitch angles, ranging from 5 to 15 degrees in 5-degree increments, and subsequent drop tests, will be integrated to enhance the understanding of the Flying-V's crashworthiness.

IV. Modelling Approaches

The analysis progresses into more dynamic scenarios, necessitating an extension of the computational domain for a more reliable study. To achieve this, enhanced finite element models will be employed to assess the crashworthiness of the Flying-V under more complex crash scenarios.

A. Baseline Model

A reference section using the best design concept was created by Desiderio et al. [2, 3]. The primary objective of Desiderio et al. design was to minimize the averaged DRI that considered the contribution of every passenger. The best-performing Flying-V design concept that is adopted as the baseline model for the present study is illustrated in Figure 9, which achieved an averaged DRI of 18.2 units. This model was constructed using 3DExperience software, where each point represents a passenger, and the color coding indicates different structural components.

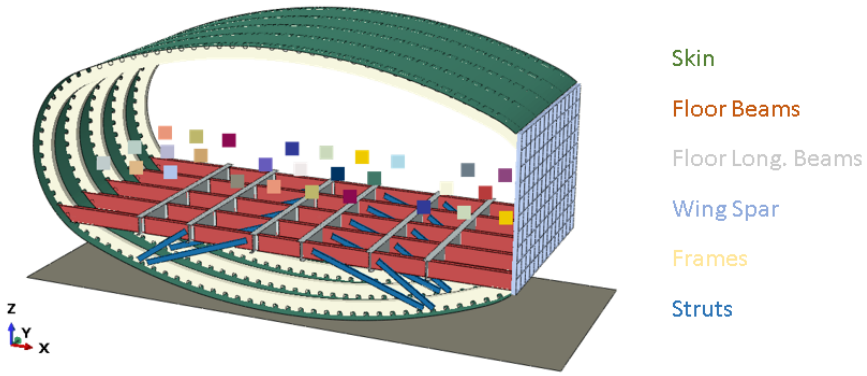

Fig. 9 Baseline model for the Flying-V fuselage. Different colors are used to identify the different structural components.

However, the adoption of the averaged DRI does not show how the spatial positioning of passengers influences the DRIs or the severity indices, making it harder to assess the influence of distinct impact scenarios over different regions of the fuselage. Therefore, to address this limitation, the plot seen in Figure 10a is constructed, where each passenger is represented by a unique identification using their seat row number and column letter.

After extracting the accelerations for each passenger (upon performing a vertical drop test with the stipulated vertical velocity) and calculating the SEVs, the resulting spatial variation and box plot are generated, as shown in Figure 10b, with different colors depicting the extent of the SEVs. As observed, the SEV values are smaller at the center, increasing towards the sides. This spatial variation in SEVs is intuitively attributed to the larger crumple zone of the center, accommodating more plastic deformation of the underlying structural elements. At the sides, there is a notable increase in structural stiffness and more direct effect of the impact waves, resulting in reduced deformations and larger peaks of acceleration on the passengers, leading to increased relative displacement of the lumbar region, according to Equation 3, which reflect on the larger DRI and consequently SEV values.

Additionally, a decrease in SEV is observed from the front to the rear part, which is attributed to the fuselage section's crushing and twisting behavior. This involves upward folding frames towards the central floor longitudinal beam.

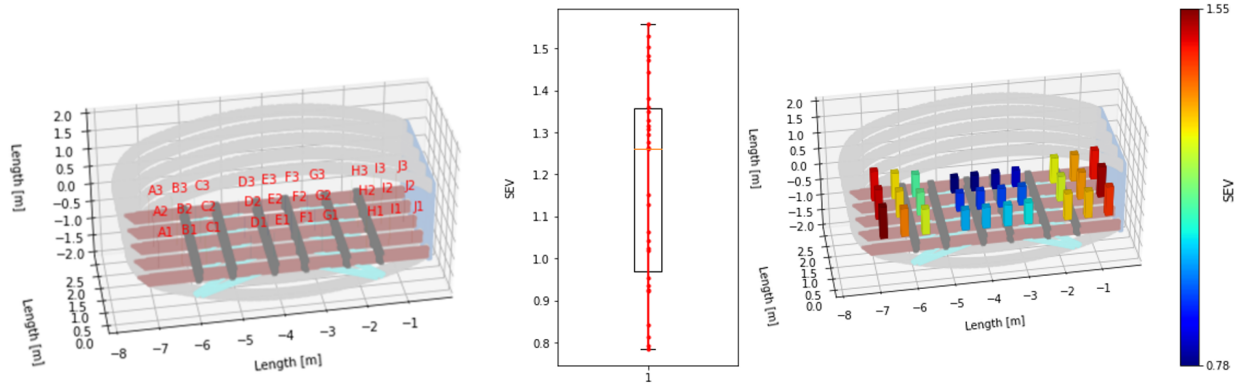

(a) Labels indicating the positions of passengers **(b) Spatial variation of the SEV**

Fig. 10 Plots of the baseline model.

B. Extended Model

As the analysis progresses into more dynamic scenarios, extending the computational domain becomes essential for a more representative study. Therefore, the baseline model is extended to double its longitudinal size. After performing a vertical drop test at 7.92 m/s, the resulting displacement and SEV variations for the extended model are shown in Figure 11. Again, higher deformations are observed at the rear part, attributed to an uneven distribution of weight

along the fuselage section. This indicates that more energy is being absorbed by the structural components, leading to reduced passenger injury towards the rear part. Besides the center of mass being shifted more towards the rear, the lateral contractions and expansions on the free edges may also contribute to the asymmetrical deformation conditions.

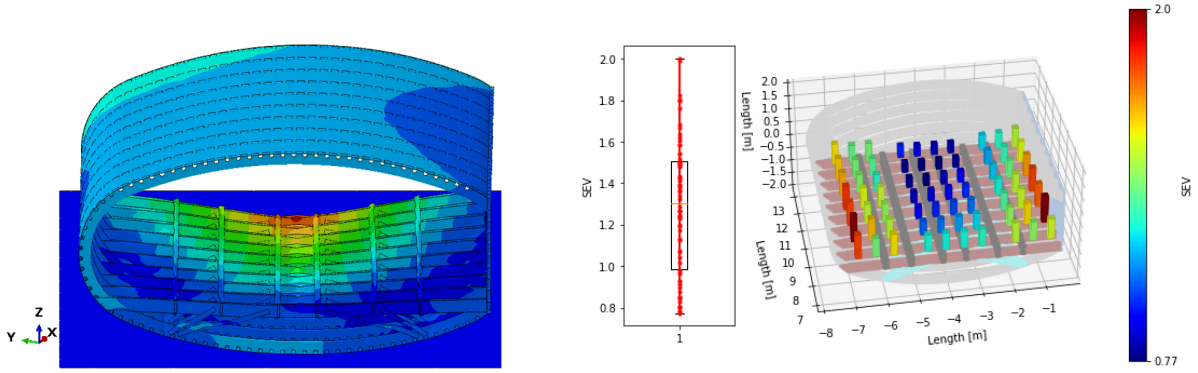

(a) Displacement variation **(b) Spatial variation of the SEV**

Fig. 11 Extended model's data from vertical drop test.

According to Dotman's work on structural sizing methodology for the fuselage of the Flying-V [1], tensile stresses are higher in the outer skin and spar, whereas compressive stresses are higher in the floor structure, leading to an asymmetric hourglassing effect, causing a change in angle about the y-axis. Effectively resisting this hourglassing requires constraining out-of-plane deformation in the longitudinal direction (y-axis) at the free edges and ensuring that all edges lie on a single contraction plane. To accomplish that, adjacent structural elements can be added, leading to the creation of the full fuselage model.

C. Full Passenger Fuselage Model

Building upon the extended model, two similar fuselage sections can be added to create the full passenger section. This model consists of three main sections: front, engine and rear. Tie connections are used to attach each section together, as depicted in Figure 12 by the different color codes.

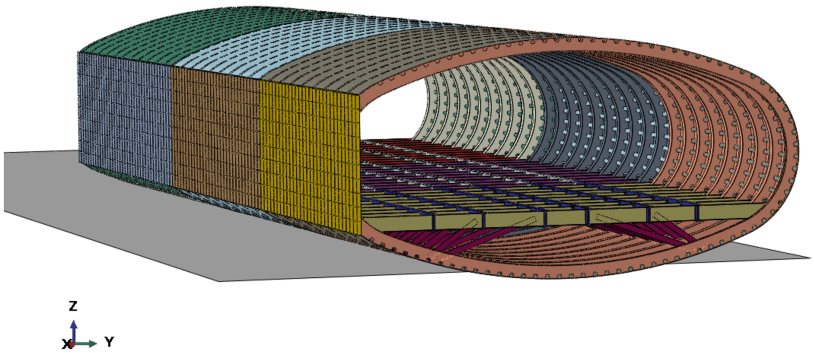

Fig. 12 Whole passengers' fuselage section.

The post-impact and subsequent injuries sustained by every passenger for the full passenger section are illustrated in Figure 13. The plastic deformation of the floor remains more or less constant from both the front and rear towards the center, gradually diminishing from the sides to the middle. Furthermore, there is again a clear trend of larger SEVs from the center to the sides.

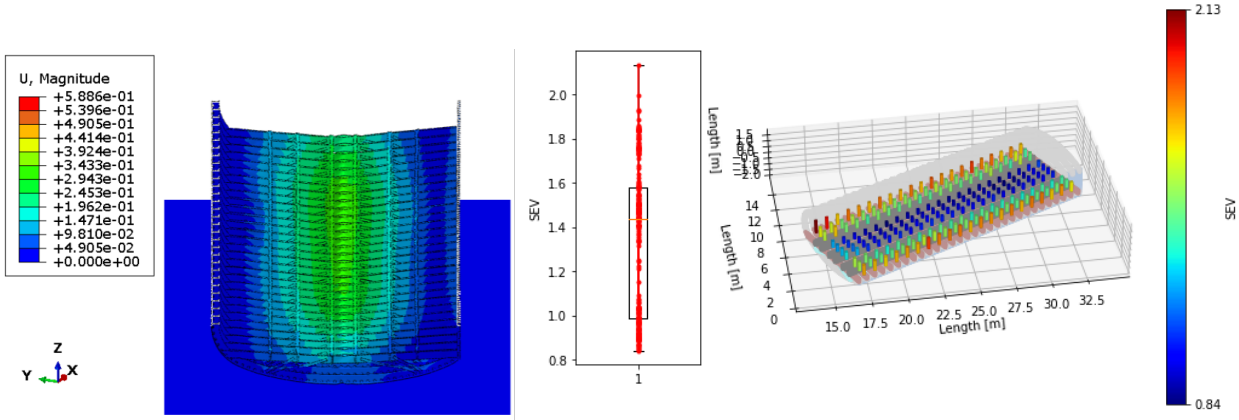

(a) Displacement variation **(b) Spatial variation of the SEV**

Fig. 13 Full passenger model's data from vertical drop test.

D. Vertical Drop Test: A Comparative Assessment

As illustrated earlier in Figure 11, the extended model demonstrated pronounced deformation at the rear part. However, when considering the engine section of the full passenger fuselage, which mirrors the extended model, the patterns of longitudinal deformation have been significantly reduced (Figure 14) by limiting the lateral contractions and expansions at the free edges, which had previously caused unrealistic out of the plane displacements. With this, a more uniform longitudinal variation of the displacement and SEVs could be achieved, providing a more accurate evaluation of the Flying-V's crashworthiness.

The full fuselage section, which is three times the length of the extended fuselage, showed a slight increase in SEVs. Despite this, it is assumed in the present work that the larger finite element model provides the most realistic results, offering a crucial reference model for the next investigations of the Flying-V under various Flying-V crash scenarios. Furthermore, the larger finite element model serves as verification for upcoming reduced modeling techniques herein investigated.

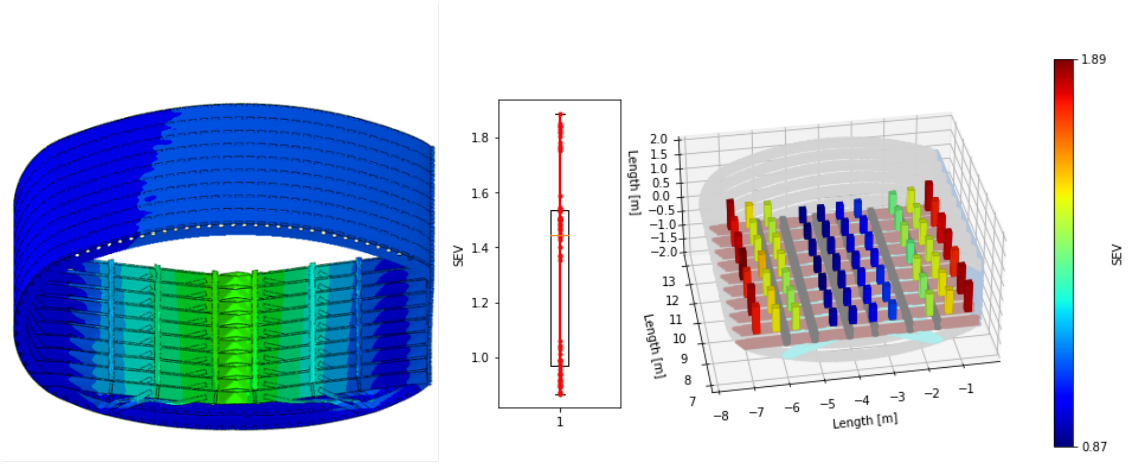

(a) Displacement variation **(b) Spatial variation of the SEV**

Fig. 14 Data from the engine section within the entire fuselage of the passenger compartment upon performing a vertical drop test.

V. Modelling Unique Flying-V Crash Scenarios

The unconventional design and mass distribution of the Flying-V complicate the assessment, making it clear that relying solely on conventional drop tests does not provide sufficient information to deem the fuselage section crashworthy. To that extent, the challenge of assessing the Flying-V's crashworthiness under alternative crash scenarios will be addressed.

Nonetheless, a thorough examination would ideally encompass the finite element model of the entire aircraft structure, but this approach introduces several challenges. Initially, only the baseline section was considered, which was subsequently expanded to include the full passenger fuselage. Despite this enlargement, the representation of the Flying-V remains incomplete, complicating an accurate crashworthiness evaluation.

Furthermore, the absence of a complete model, coupled with missing moments of inertia for other sections, could lead to rotational issues and unrealistic results. Therefore, addressing these gaps is essential for ensuring a reliable assessment of the Flying-V's crashworthiness across various impact scenarios.

A. Simplified Modelling Techniques: Introducing the Implicit Moments of Inertia Approach

To address these challenges without constructing a comprehensive full FEM model, a strategy involving further manipulation of existing resources is developed. The fuselage section maintains consistency along the longitudinal axis from the nose section to the outer wing, as seen in Figure 15. This section is extended beyond the full passenger model to encompass the entire fuselage using 3DExperience, which facilitated the computation of weight and moments of inertia for each segment through the application of Class III methods.

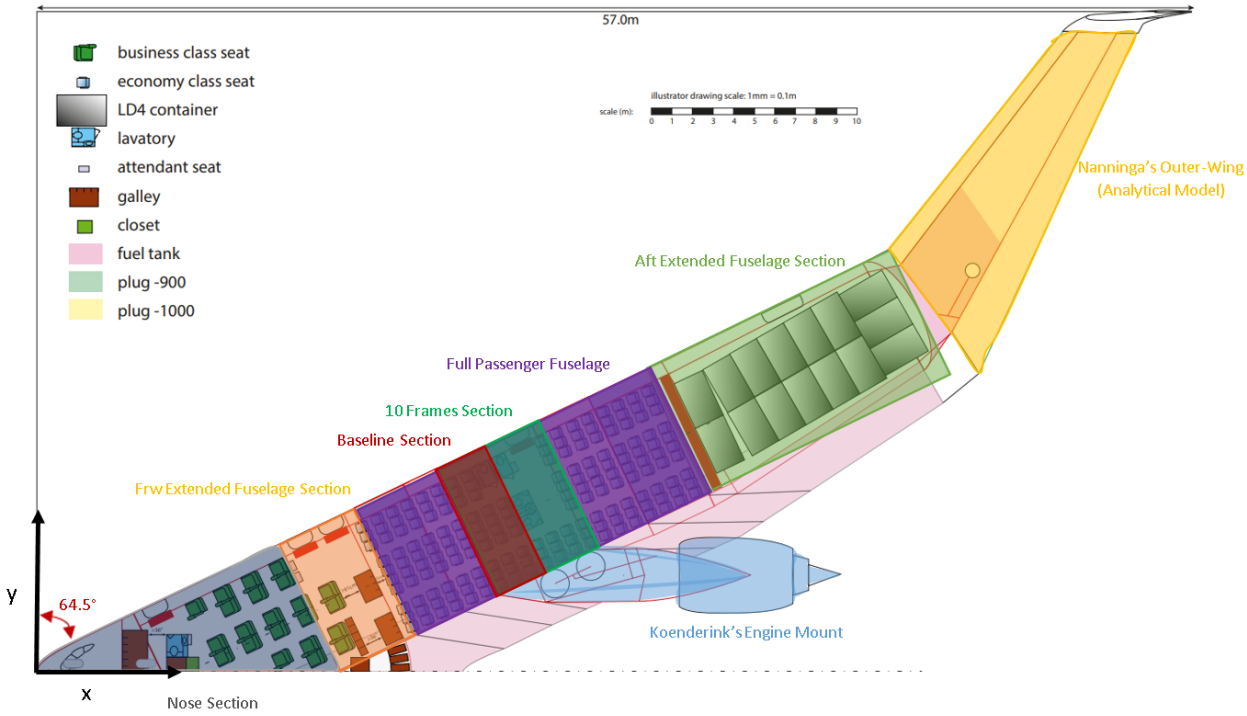

Fig. 15 Proposed Part Subdivision for the Flying-V.

For the nose section, a rough estimate is conducted. Recognizing the significance of mass and moments of inertia for this study, the fuselage forward section is extended until the origin of the global coordinate system (see Figure 16a), followed by making a cut along the global x-direction, leading to the creation of the model depicted in Figure 16b.

The outer wing depicted in yellow in Figure 15, is treated as a normal wing with an airfoil shape of constant density, and analytical methodology is proposed to calculate its center of gravity and moments of inertia, as detailed in the Appendix F of reference [22].

While the finite element method models created and the analytical methods used for the outer wing were rudimentary, a nearly comprehensive FEM model of the Flying-V was developed. The primary weight of each fuselage part was

determined directly from 3DExperience software, along with the respective moments of inertia about their centers of gravity.

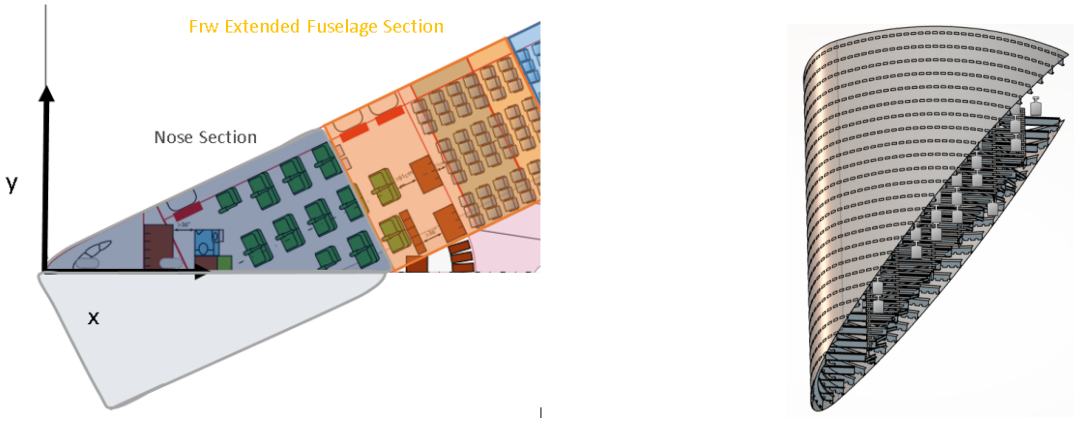

(a) Fuselage extension. The shaded part was removed **(b) FEM model of the nose section**

Fig. 16 Nose section development process.

The model is simplified by utilizing the previously estimated inertia properties for the various parts of the Flying-V, and condensing the corresponding sections into two singular points (Figure 17), encompassing their cumulative inertial properties using the principles of superposition and the parallel axis theorem. These moments of inertia at designated reference points facilitated distributed coupling between the reference points and cross sections of the extended Flying-V section, allowing for natural deformation of secondary nodes and preserving the authenticity of the simulation. It is worth noting that only inertias were incorporated into the model, while the mass was omitted to prevent potential acceleration increases without accounting for the crash dynamics and energy absorption by other component representations. By using the inertial properties of the other sections, a rough estimation of the dynamics and handling characteristics of the aircraft can be achieved, providing valuable insights into its crashworthiness.

B. Optimizing Vertical Drop Tests for the Flying-V: Leveraging Moments of Inertia

The validity and effectiveness of the proposed implicit moments of inertia approach can first be verified through conventional drop tests using the extended model. Figure 17 illustrates the extended section with moments of inertia at reference points attached to the cross sections.

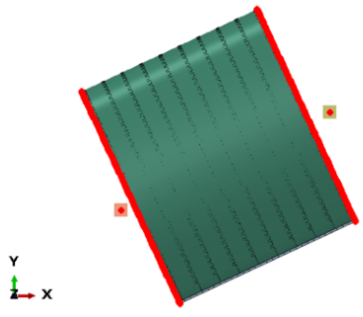

Fig. 17 Top view of the extended fuselage section.

Upon analyzing the displacement and SEV variations shown in Figure 18, it is evident that the previously observed deformations at the rear part (Figure 11a) have been reduced, leading to a more uniform SEV distribution along the longitudinal axis. These findings more closely align with the results from the engine section of the full passenger model (Figure 14).

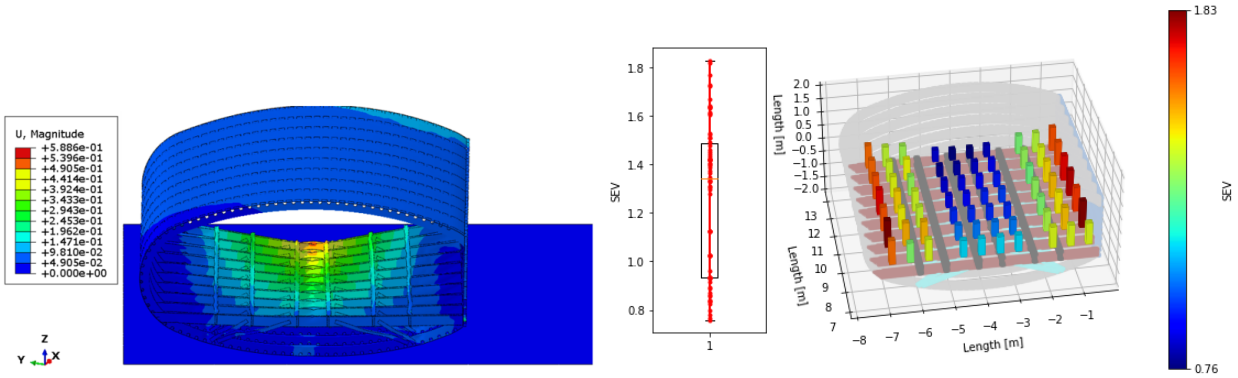

(a) Displacement variation **(b) Spatial variation of the SEV**

Fig. 18 Data of the extended model with moments of inertia applied, upon performing vertical drop test.

By introducing additional momentum representative of other sections of the Flying-V to the free edges of each cross section, the kinematic behavior induced by subsequent parts is effectively conveyed to the extended section, eliminating the need for a fully representative model.

Furthermore, there are notable outcomes in terms of computational efficiency. Incorporating moments of inertia into the extended model significantly reduces the simulation time for the corresponding sections, almost halving it. This is consistent with expectations, as fewer floor deformations lead to a faster solver solution.

Models	SEV				Comp. Time
-	Avg	Max	Median	Min	(h)
Ext. 7 rows	1.29	2.00	1.30	0.77	6.54
Ext. 7 rows Inertia	1.27	1.83	1.34	0.76	3.83
Full Model Eng. Section	1.33	1.89	1.44	0.87	-

Fig. 19 Differences in computational time.

C. A Preliminary Analysis: Counteracting the Engine Weight

Following the evaluation of the proposed methodology for vertical drop tests, the next step is to test this approach by introducing the engine weight and engine mount representation attached to the middle extended section. The engine and landing gear mounting structures were designed by Koenderink [23], who also estimated the mass to be approximately 22,150 kg, including the landing gear and engine. In contrast, the structural mass of the extended fuselage section, even when including the mass of each passenger and seat, amounts to 7,080 kg.

Two simulations were conducted, one with and another without the inclusion of the moments of inertia. The behavior of the section in these scenarios is shown in Figure 20. It can be seen that when the moments of inertia from other sections are considered, the rotation induced by the engine's weight was effectively and more realistically countered. Without the moments of inertia of the adjacent structures, however, the structure rotates backwards, influenced by the large momentum of the engine mounting structures. This initial analysis, coupled with insights from the preceding section, offers a promising evaluation of the proposed simplified methodology. The results demonstrate that incorporating moments of inertia not only enhances the accuracy of the simulation but also reduces its computational time, leading to more realistic and reliable crashworthiness assessments.

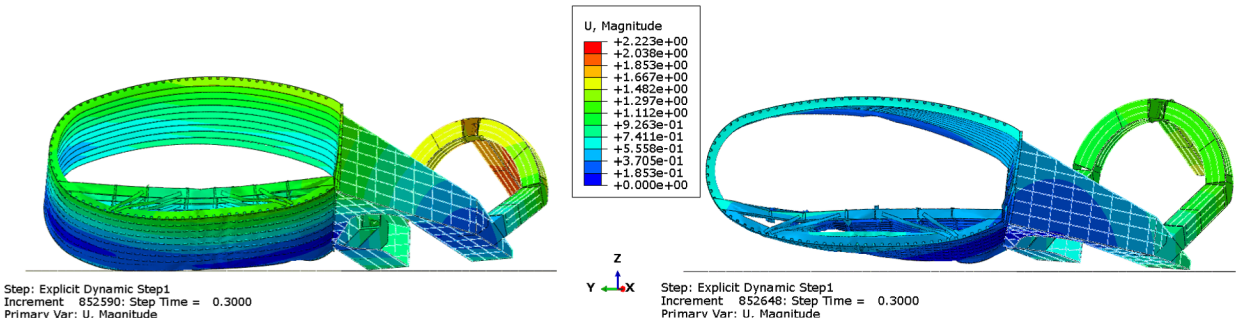

(a) Model's deformed state without considering moments of inertia of other sections of the FV

(b) Model's deformed state when moments of inertia of other sections of the FV are considered

Fig. 20 Impact of adding moments of inertia from other segments of the Flying-V.

D. Effect of Roll Angles on the Flying-V Fuselage Crashworthiness

Following the positive results from previous analyses, it was considered advantageous to further use the extended model including moments of inertia of the adjacent structures as boundary conditions, to assess the crashworthiness of the Flying-V under different roll angles. Drop tests with 5-degree, 10-degree, and 15-degree roll angles were evaluated, all featuring the same vertical impact velocity of 26 ft/s (7.925 m/s). The stress variations observed in these tests are depicted in Figure 21, with the same frame analyzed for each drop test.

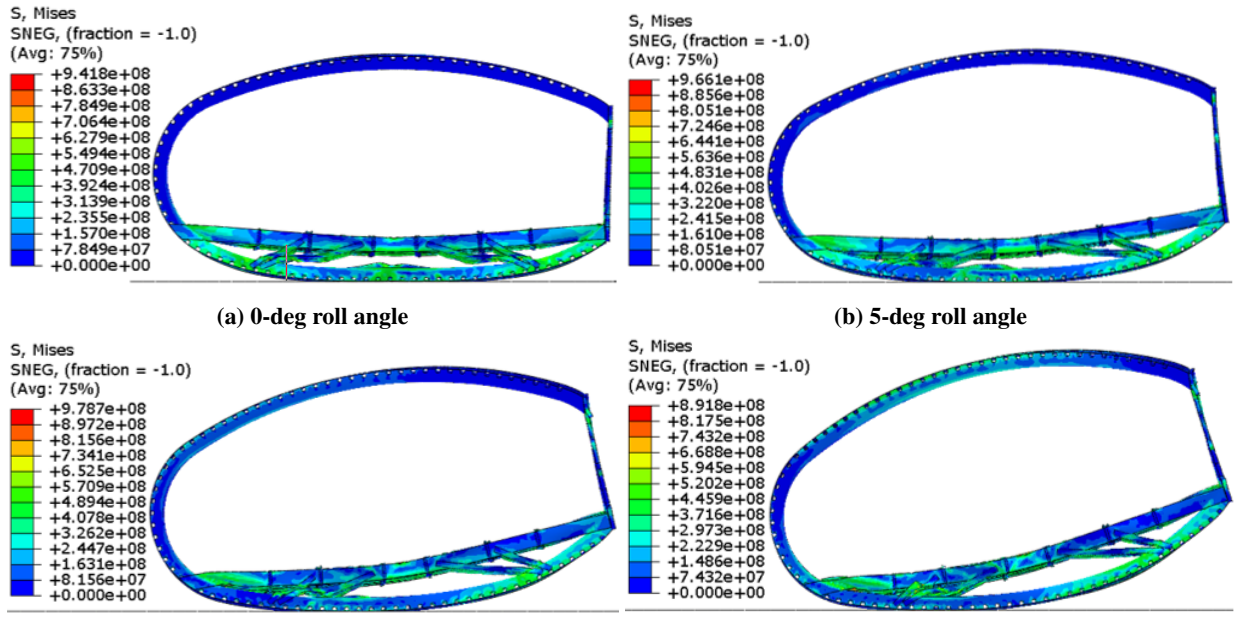

(a) 0-deg roll angle

(b) 5-deg roll angle

(c) 10-deg roll angle

(d) 15-deg roll angle

Fig. 21 Deformation and stress variation of fuselage section at 75 ms.

Whereas fuselage frames were previously the primary energy absorption components in perpendicular impact cases, the introduction of roll angles redirected more energy absorption towards floor components, as shown in Figure 22, leading to higher plastic deformation.

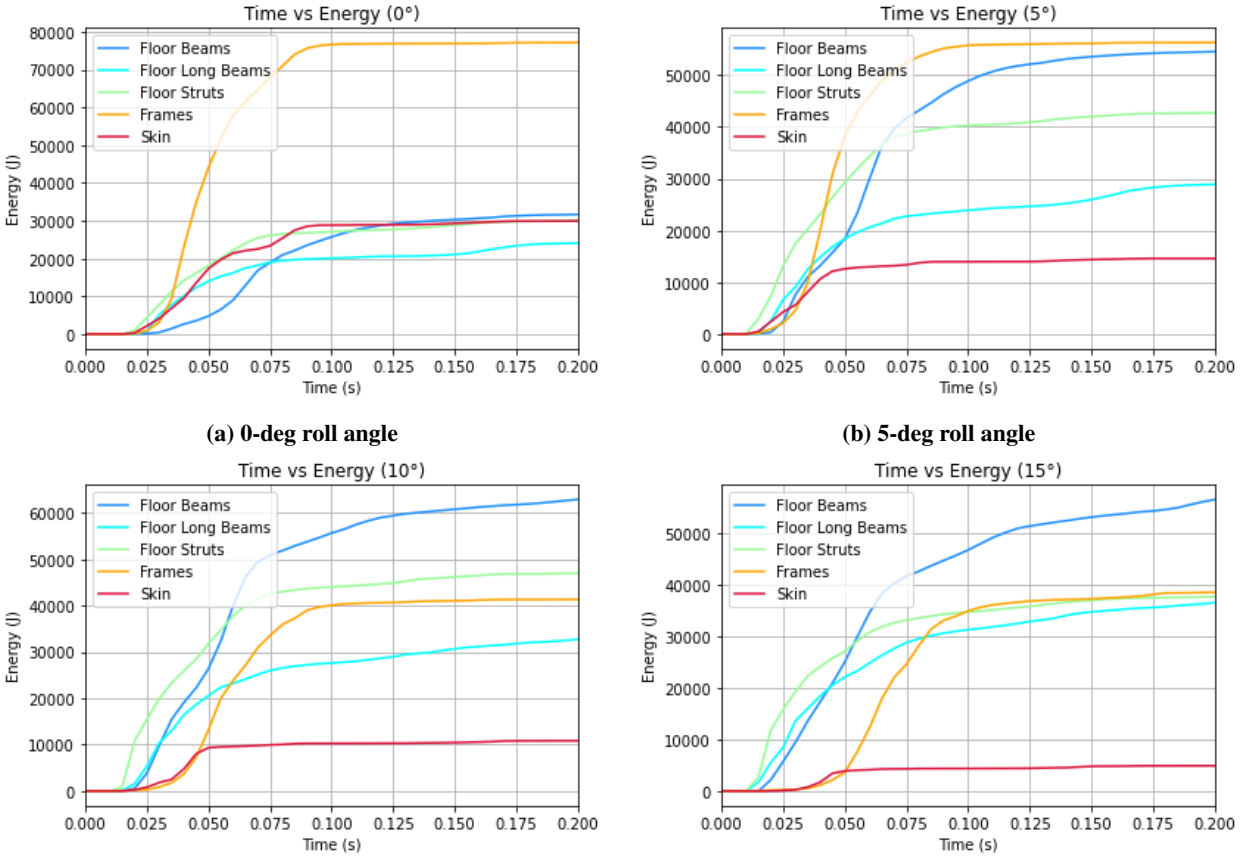

(a) 0-deg roll angle

(b) 5-deg roll angle

(c) 10-deg roll angle

(d) 15-deg roll angle

Fig. 22 Energy absorption of main structures of fuselage section with different roll angles.

This shift of energy absorption towards floor structures raise significant concerns in maintaining occupants' egress paths, one of the main criteria related to crashworthiness. Additionally, the floor struts, located directly above the impact area when roll angles are introduced, function as the primary energy-absorbing structure during the initial impact stages, contributing to higher SEV values observed on the left side compared to the right side (Figure 23). The introduction of roll angles causes the section to impact a more localized region, particularly on the left side, inducing high accelerations for passengers above the initial crash region.

These observations yield both favorable and unfavorable outcomes: the introduction of roll angles can elevate the risk of injury to passengers directly above the point of impact. This localized impact initiation concentrates stress in a smaller region, resulting in higher SEVs, which could prove fatal in extreme cases. Conversely, passengers farther away from the impact area experience increased chances of survival.

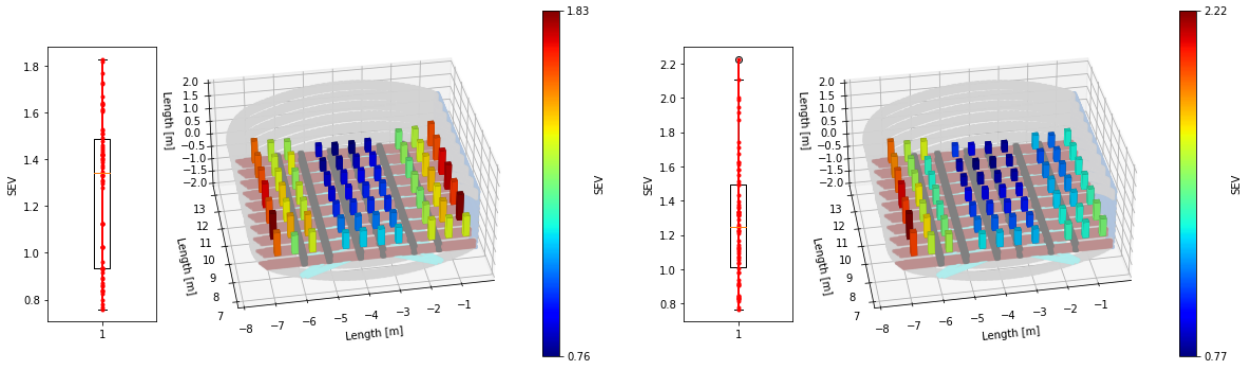

(a) 0-deg roll angle

(b) 5-deg roll angle

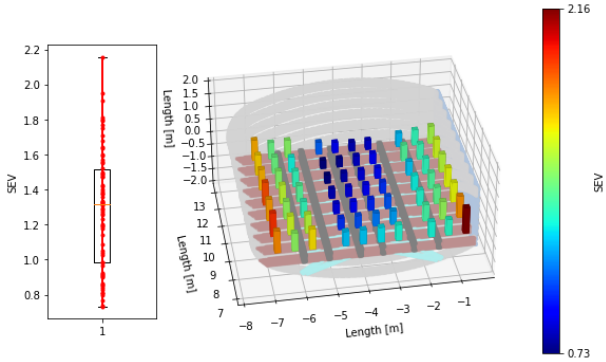

(c) 10-deg roll angle

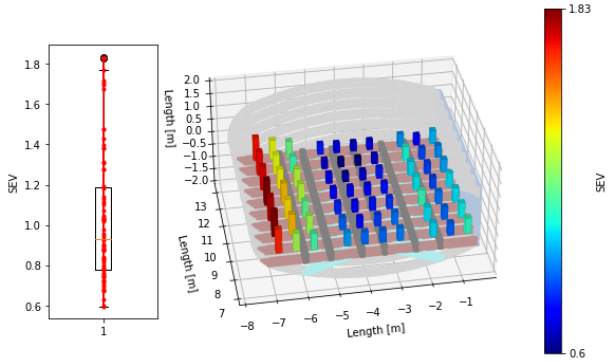

(d) 15-deg roll angle

Fig. 23 Spatial variation of the SEV with different roll angles.

E. Effect of Pitch Angles on the Flying-V Fuselage Crashworthiness

In all previous analyses, the centerline of the sections being analyzed maintained a horizontal orientation. For these cases, the implicit moments of inertia presented positive outcomes. However, other crash scenarios involve varying centerline orientations, particularly pitch angles that lead to rigid body rotation upon impact. This behavior can occur, for example, during a tail-first impact, where the fuselage section of the Flying-V is likely to undergo significant rigid-body rotation when the wingtips make contact with the ground.

To assess the crashworthiness of the Flying-V under these conditions, pitch angles of 0, 5, 10 and 15 degrees are investigated, with a vertical impact velocity of 26 ft/s (7.925 m/s). For these simulations the most complete model available is used, namely the full passenger fuselage. Subsequently, the same cases are simulated with the extended model using the moments of inertia boundary conditions, with the aim to verify the previously proposed methodology for cases of non-zero pitch angle.

The frame analyzed in Figure 24 corresponds to 0.1 seconds, which is the point of maximum deformation for the perpendicular drop test. In this scenario, the impact area involves the full lower frames and reinforcements. Conversely, increased pitch angles cause more localized impact initiations in smaller areas, leading to increased stresses.

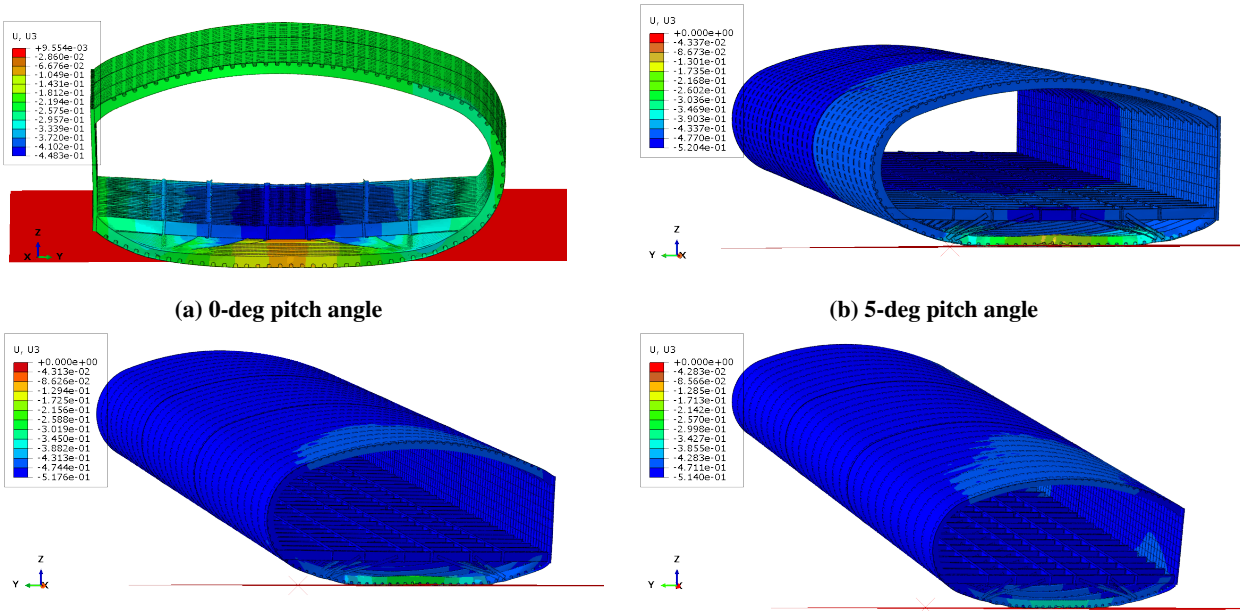

(a) 0-deg pitch angle **(b) 5-deg pitch angle**

(c) 10-deg pitch angle **(d) 15-deg pitch angle**

Fig. 24 Displacement magnitude with different pitch angles.

Higher pitch angles also increases the kinetic energy of the model (Figure 25), boosting angular momentum and resulting in higher impacting forces, particularly in regions farther from the rotation point.

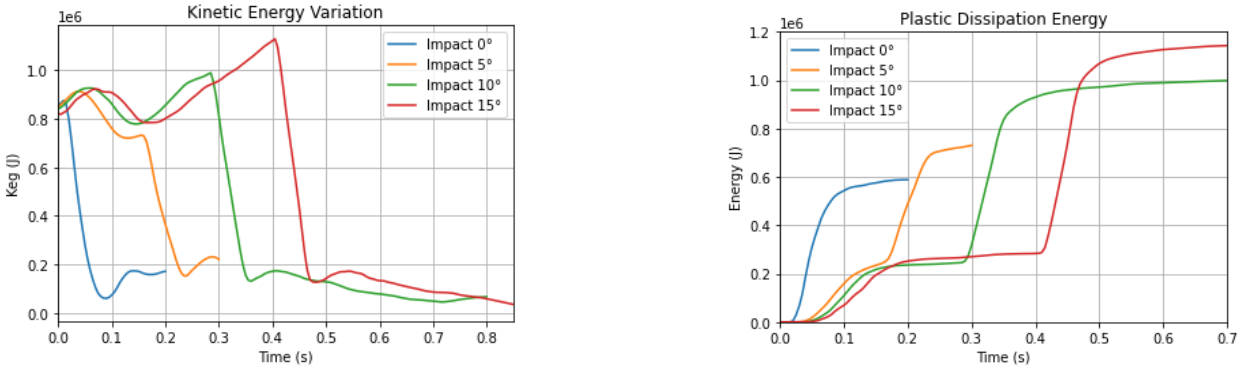

(a) Kinetic energy history **(b) Plastic dissipation energy history**

Fig. 25 Energy histories of fuselage sections with different pitch angles.

The subsequent deformation patterns contrast with previous results, causing elevated SEV values in the middle longitudinal areas rather than near the spar and lateral frames, especially at the fuselage's rear end, as illustrated in Figure 26. The very high velocities at the section's end result in strong impact forces and significant deformations of structural elements. The limited space between frames and the floor structure cannot contain the large plastic deformations, ultimately impacting floor structural elements and subjecting passengers to excessive accelerations.

The elliptic shape of the Flying-V cross section poses additional challenges, providing less crushing distance. Additionally, the first row for cases of non-zero pitch angles exhibits higher SEV values due to the impact initiation in a small area, consistent with previous observations.

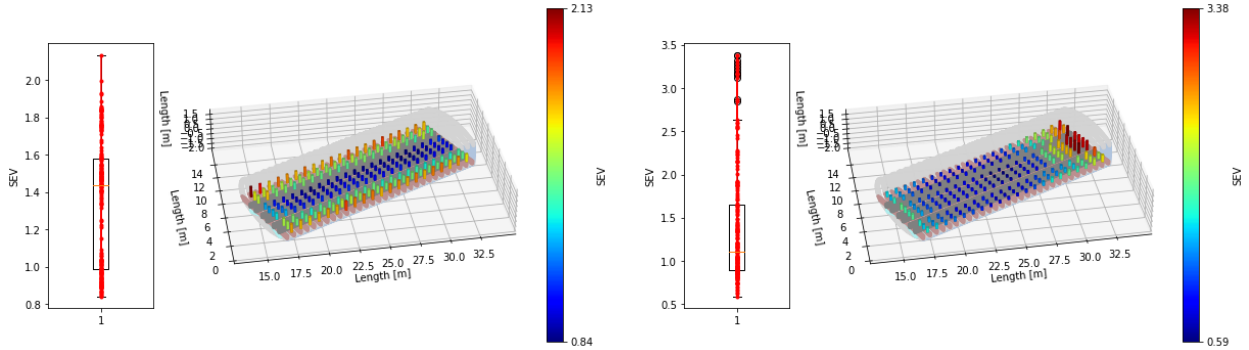

(a) 0-deg pitch angle

(b) 5-deg pitch angle

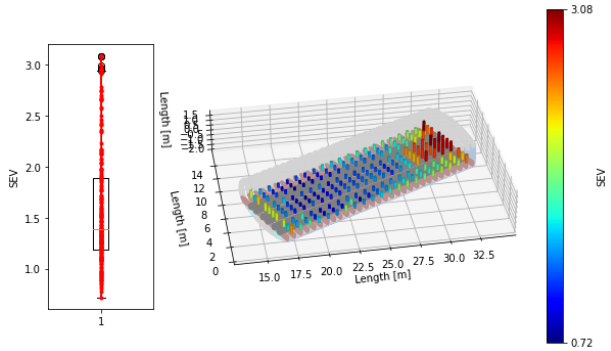

(c) 10-deg pitch angle

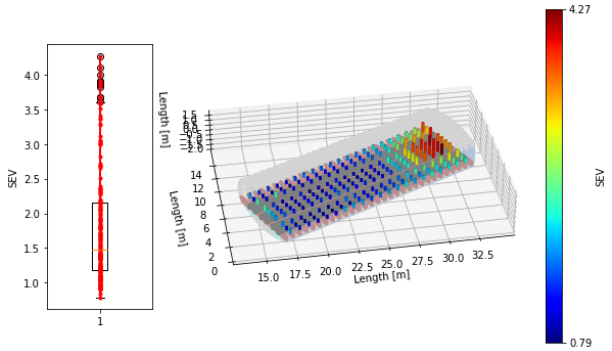

(d) 15-deg pitch angle

Fig. 26 Spatial variation of the SEV with different pitch angles.

F. Reduced Model Analysis: An Assessment of the Viability of the Implicit Moments of Inertia Technique

After evaluating the crashworthiness of the entire passenger fuselage under various pitch angles, the next phase involves assessing the practicality of the previously suggested simplified modeling technique. In this scenario, the same methodology is employed, utilizing the extended model positioned near the fuselage's midsection. The moments of inertia of the front and rear sections of the passenger fuselage are then applied to their corresponding reference points.

Due to the reduced length of the extended model compared to the full passenger fuselage — approximately three times smaller — a straightforward introduction of a pitch angle cannot be conducted for the reduced model and the associated drop tests. To overcome this challenge, a new validation approach was implemented.

1. Validation Approach

To calculate the analytical velocities upon impact for crash scenarios with different pitch angles, a rigid body rotation of the entire passengers'fuselage was taken into account, revolving around a point of contact with the ground. For clarity and precision, three distinct states were delineated to capture the dynamics of the impact scenario:

- State 1: This represents the moment just before the passenger fuselage makes contact with the ground, with a specific pitch angle incorporated into its orientation (see state 1 in Figure 27);
- State 2: This signifies the moment immediately after the passenger fuselage comes into contact with the ground (state 2 in Figure 27);
- State 3: This denotes the moment just before the entire fuselage touches the ground, now in a parallel orientation to it (state 3 in Figure 27).

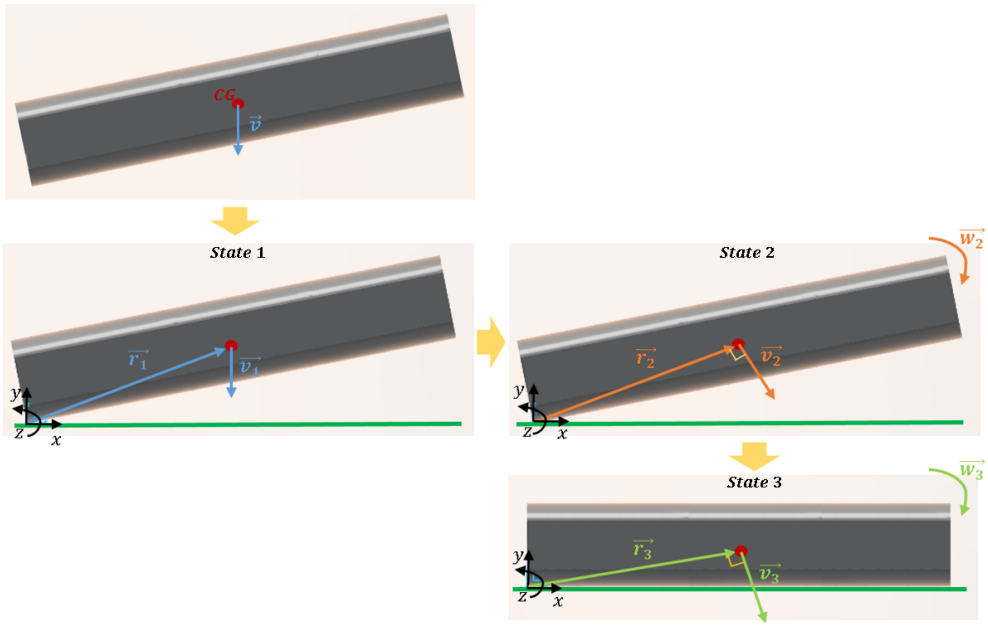

Fig. 27 All the steps considered in the rigid body rotation of the passengers' fuselage.

Between States 1 and 2, the impact was treated as perfectly plastic, with angular momentum conservation applied:

$$\vec{H}_{O_1} = \vec{H}_{O_2} \Leftrightarrow$$

$$(\vec{r}_1 \times \vec{v}_1)m + \mathbf{I}_{CG} \cdot \vec{w}_1 = (\vec{r}_2 \times \vec{v}_2)m + \mathbf{I}_{CG} \cdot \vec{w}_2 \tag{5}$$

where $\vec{r}_1 = \vec{r}_2$ and $\vec{w}_1 = 0$, due to zero body's rotation in the initial state. The distances $\vec{r}_1$ and $\vec{r}_2$ between the point of contact and the center of gravity (CG) of the passengers' fuselage for various pitch angles were considered. These values, along with mass and inertia matrices, were directly extracted from the 3DEXPERIENCE platform.

Subsequently, by substituting these values into Eq. 5 and using the relationship $\vec{v} = \vec{r} \times \vec{w}$, the angular velocity $\vec{w}_2$ was determined for various pitch angles. This, in turn, allowed for the calculation of $\vec{v}_2$ for the respective pitch angles.

Moving from States 2 to 3, the conservation of energy was invoked to analyze the distribution of kinetic and potential energy:

$$T_2 + \sum U_{2\to3} = T_3 \Leftrightarrow$$

$$\frac{1}{2}m\vec{v}_2^2 + \frac{1}{2}\vec{\omega}_2^T\mathbf{I}_{CG}\vec{\omega}_2 + \Delta y\, mg = \frac{1}{2}m\vec{v}_3^2 + \frac{1}{2}\vec{\omega}_3^T\mathbf{I}_{CG0}\vec{\omega}_3 \tag{6}$$

This allowed for the determination of the variation in height, y, between the perpendicular orientation of the fuselage to the ground and its corresponding pitch angle.

Finally, the velocities were calculated for the center of gravity of the full passenger model. It's important to note that the center of gravity of the full passenger model may not coincide with that of the reduced model. However, due to the uniform circular motion of the model, it was reasonable to assume that the angular velocity of the reduced model, $\vec{\omega}_{red}$, is equal to $\vec{\omega}_3$. Utilizing this information, along with the center of gravity of the reduced model extracted directly from the 3DEXPERIENCE platform, the final velocity components upon impact could be determined.

2. Visual Inspection of the Crash Scenarios

The calculated velocities were applied to the model, and subsequent drop tests were conducted, revealing significant insights into crash behavior under maximum deformation, as seen on the left side of Figures 28, 29 and 30. On the right side, similar drop tests with the engine section of the full passenger model are depicted for comparison.

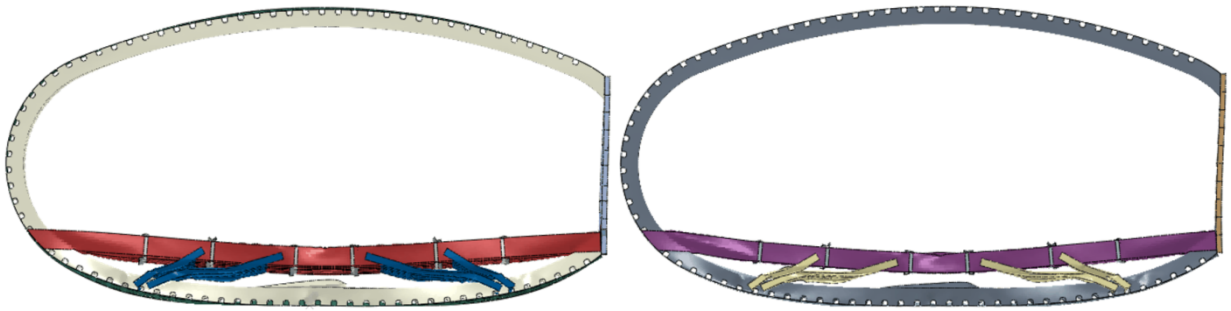

(a) Maximum deformation of the reduced model **(b) Maximum deformation of the engine (extended) section**

Fig. 28 Maximum deformation for the perpendicular impact cases.

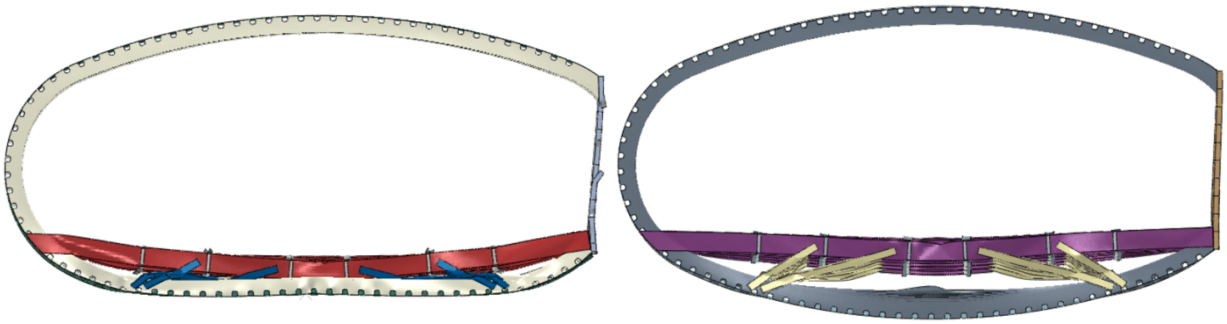

(a) Maximum deformation of the reduced model **(b) Maximum deformation of the engine (extended) section**

Fig. 29 Maximum deformation for the 5 degrees impact cases.

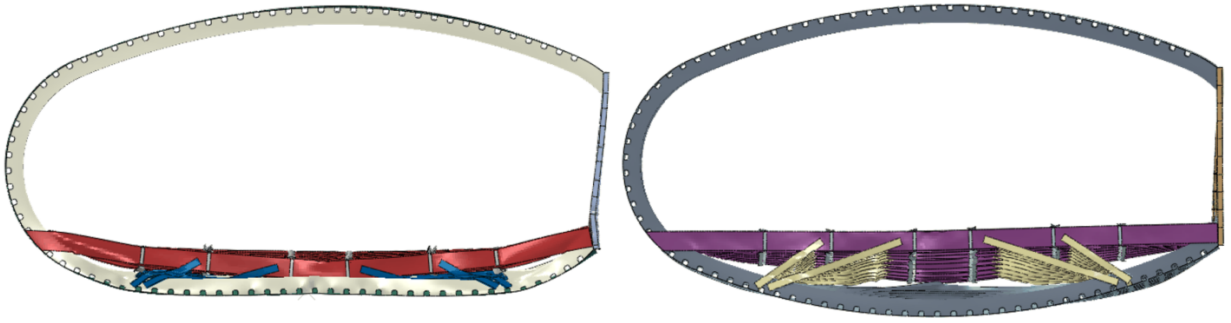

(a) Maximum deformation of the reduced model **(b) Maximum deformation of the engine (extended) section**

Fig. 30 Maximum deformation for the 10 and 15 degrees impact cases (both deformations were very similar).

For the 0 degrees case, only the moments of inertia of the rear and front sections of the passenger fuselage were considered. This approach showed a trend consistent with the engine section of the full passenger model, affirming the efficacy of using moments of inertia for straightforward vertical drop tests. However, when introducing a pitch angle and corresponding analytical velocity upon impact for the reduced model, the crash sections displayed markedly different characteristics. Deformations were significantly greater compared to the full fuselage section. This outcome was somewhat anticipated due to the simplified methodology, which only accounts for moments of inertia without considering mass. While this approach captures the kinematics to some extent, it lacks physical representation, resulting in zero absorption of impact energy by the rear and front sections.

The SEV analysis depicted in Figures 31, 32, and 33 for the different pitch angles supports these findings.

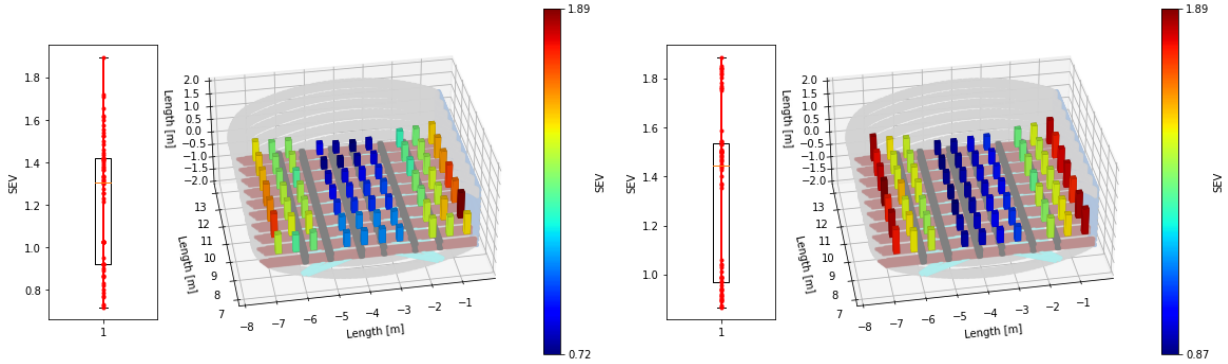

(a) Reduced/extended model **(b) Engine (extended) section of the full passenger model**

Fig. 31 Spatial variation of the SEV for the 0 degrees case.

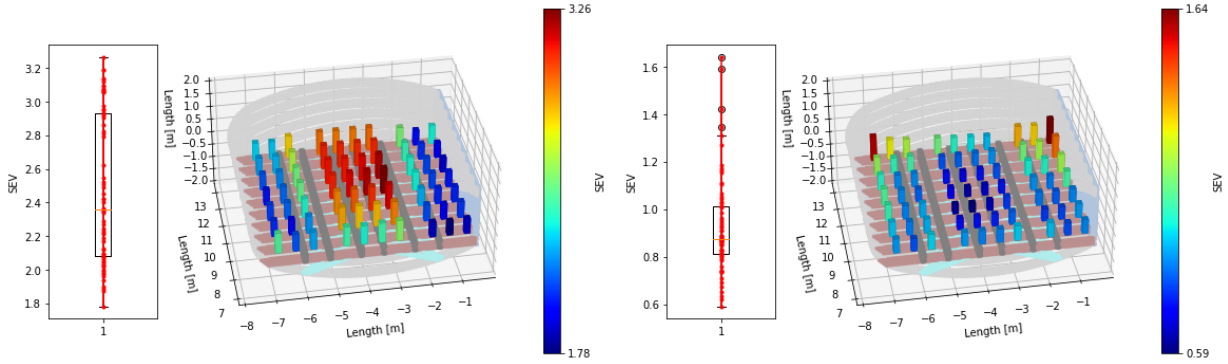

(a) Reduced/extended model **(b) Engine (extended) section of the full passenger model**

Fig. 32 Spatial variation of the SEV for the 5 degrees case.

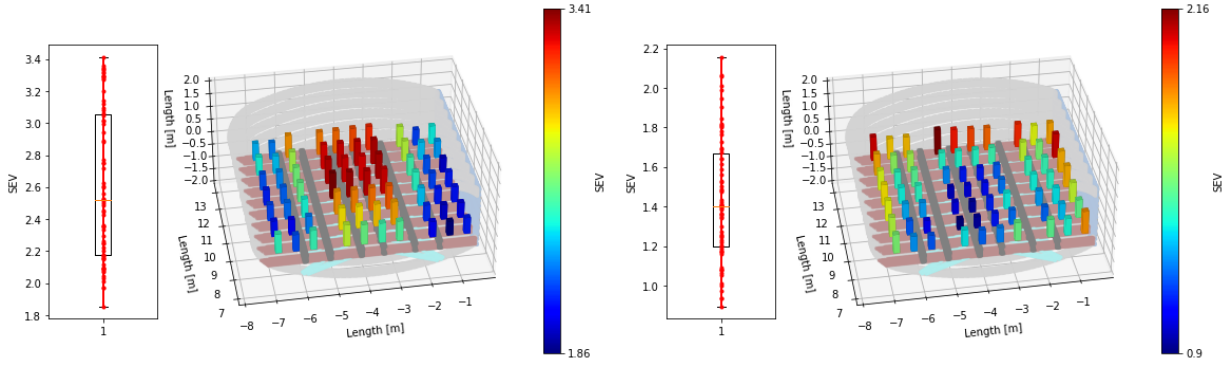

(a) Reduced/extended model **(b) Engine (extended) section of the full passenger model**

Fig. 33 Spatial variation of the SEV for the 10 and 15 degrees case. Results were deemed very similar.

In the 0-degree case, there is a commendable correlation between the Figures. The impact surface, involving lower frames and reinforcements, makes simultaneous ground contact, resulting in relatively uniform longitudinal damage. The increased plastic deformation in the fuselage's middle enhances energy absorption, leading to reduced SEV. Conversely, increased stiffness towards the sides results in less structural deformation, yielding higher SEV.

Introducing pitch angles of 5 to 15 degrees results in augmented final impact velocity, incorporating additional angular velocity from the fuselage section's rotation. This intensifies ground impacts, substantially elevating SEV values for the reduced model. The additional velocities due to pitch angles cause higher SEV values in the middle longitudinal areas rather than the sides near the spar and lateral frames. This shift arises from the exceedingly high velocities, generating robust impact forces and significant deformations of structural elements. The limited space between frames and the floor structure proves inadequate for containing extensive plastic deformations, consequently affecting floor structural elements and exposing passengers to excessive accelerations.

For the full model engine counterpart, the initial impact of the full passenger model's front section absorbs some impact energy, with the deformation peak occurring at the rear part. The middle engine section benefits from a degree of "protection" provided by the adjacent sections, resulting in modest SEVs. An increase in SEVs is only observed in the last row of the engine section, just before the rear part begins.

The significant rise in injury criteria values with increasing pitch angles for the reduced modeling technique is also closely tied to the conservation of angular momentum. In the extended model with moments of inertia, all vertical velocity is converted into angular velocity upon the first contact point. In contrast, for the full passenger case, most vertical velocity is reduced before being converted into angular velocity.

Moreover, the absence of FEM representations for the rear and front sections of the passengers' fuselage contributes to the significant discrepancy in results. Without such inclusion, these sections do not actively participate in energy absorption upon impact, deviating from the gradual energy absorption observed in the full passenger fuselage scenario. Therefore, it can be concluded that, when introducing a variable centerline orientation, the reduced modeling approach does not yield reliable outcomes.

G. Alternative Simplified Modelling Technique: Introducing Submodelling

Given the unsatisfactory outcomes from the initial methodology, an alternative approach has been proposed to better address extreme crash scenarios. This method, known as submodelling, avoids overly simplified models and refines analyses in specific areas without overwhelming computational resources.

Submodelling involves conducting an initial drop test on the entire passenger model with a substantially coarser mesh, seen in Figure 34a, effectively reducing the computational time required for the analysis. Subsequently, the same drop test is replicated using the submodelling technique, with a further refinement focused on the section of interest, in this case, the engine part (Figure 34b). The results obtained from the full model drop test are then interpolated onto the free edges of the engine model, significantly enhancing the overall precision of the outcomes. This technique was tested under the most severe drop conditions, specifically with a 15 ° pitch angle, as additional cases were deemed unnecessary to validate the effectiveness of the alternative approach.

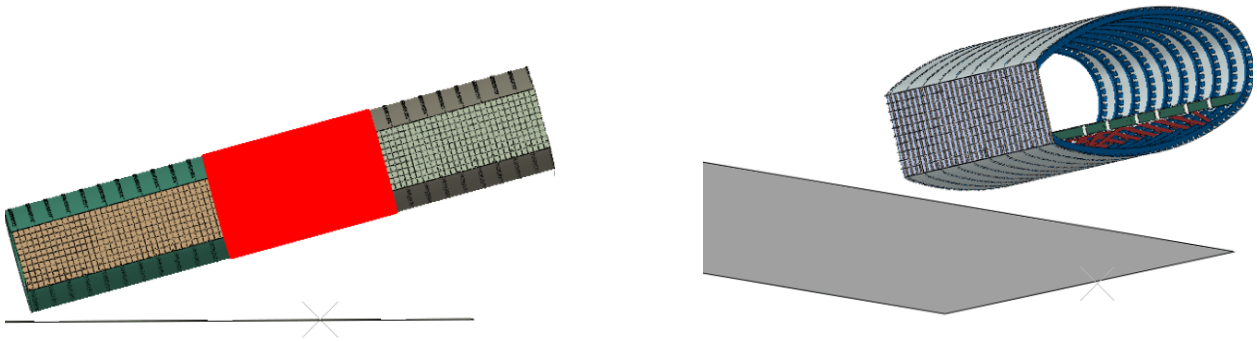

(a) Engine section location in the full passenger model **(b) Engine section used for submodelling**

Fig. 34 FEM model of the engine section and its location in the full passenger model.

Upon visually examining the crash sections generated from the drop test, depicted in Figure 35, a striking similarity emerges, with the color-coded representation aligning consistently in both simulations.

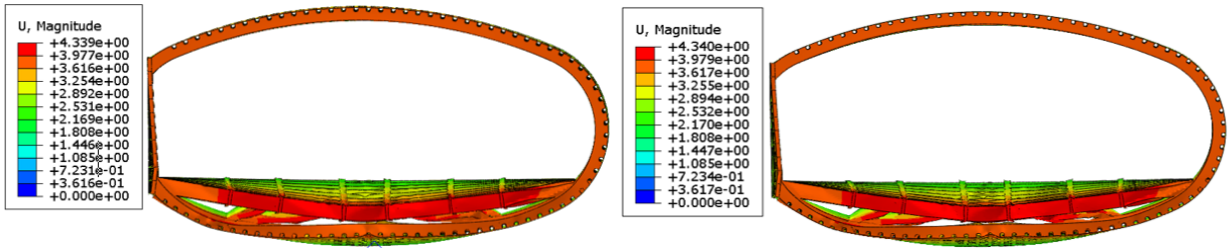

(a) Maximum deformation of the submodel **(b) Maximum deformation of the engine (extended) model**

Fig. 35 Rear views showcasing maximum deformation for the two cases (0.48s). The right one corresponds to the engine section of the full passenger model.

The similarity in results is further supported by the nearly identical spatial injury variation along the section for both cases (seen in Figure 36).

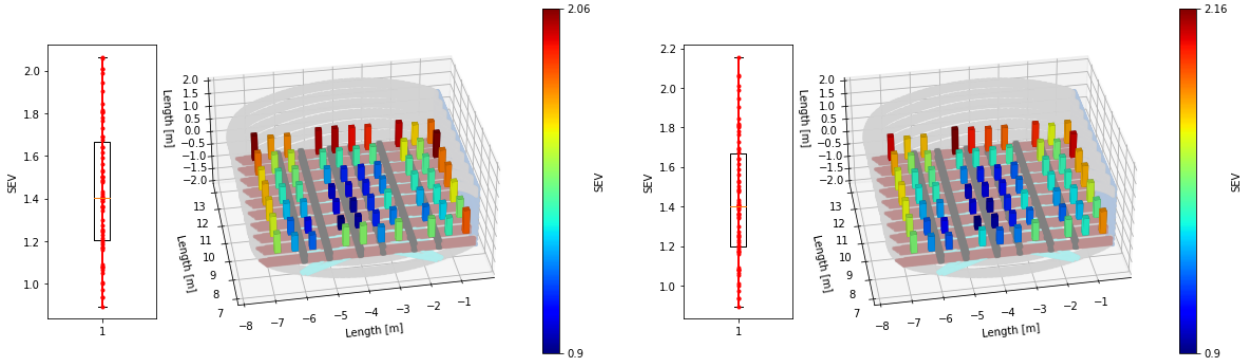

(a) Submodel **(b) Engine (extended) section of the full passenger model**

Fig. 36 Spatial variation of the SEV.

This was also achieved by nearly halving the computational time using the submodel technique compared to its counterpart (see Table 1). Notably, the computational time for the submodel already includes the duration needed to perform the full passenger drop test with a rough mesh, followed by the engine drop test with a refined mesh.

Table 1 SEV comparison for modelling techniques.

Model	Angle	SEV				Comp. Time
		Avg	Max	Median	Min	(h)
Submodel	15-deg	1.36	2.06	1.34	0.90	23.62
Engine	15-deg	1.44	2.16	1.40	0.90	44.68

While the implicit modelling technique considers the moments of inertia of all Flying-V parts, providing a rough estimation of their dynamics, its precision diminishes when conducting more complex drop tests, such as those involving pitch angles, leading to imprecise and unrealistic results. Conversely, the submodelling technique delivers high precision coupled with a substantial reduction in computational time. However, it is essential to emphasize that a comprehensive FEM representation of a more complex model is requisite before employing the submodelling technique.

VI. Conclusions

In conclusion, for vertical drop tests, incorporating moments of inertia brought the section closer to the impact behavior observed in the engine section of the full passenger model, yielding more realistic results and reducing simulation time. This approach proved effective in capturing the essential dynamics without overwhelming computational resources.

Upon introduction roll angles, there was a shifted energy absorption from fuselage frames to floor components. This shift could potentially hinder occupants' ability to exit safely after a crash. Additionally, left roll angles increased peak acceleration on the left side and decreased it on the right, raising concerns for the passengers seated above the impact zone.

The addition of pitch angles further complicated the impact dynamics. The increased angular momentum, combined with the limited space between frames and the floor structure, led to high accelerations sustained by passengers farther away from the rotation point. This raises significant safety concerns, as conventional designs with higher crushing distances may produce different outcomes. Also, the implicit modelling technique, when used for drop tests involving pitch angles, resulted in imprecise and unrealistic outcomes.

As an alternative, the submodelling technique offered higher precision with a substantial reduction in computational time. This method allowed for detailed analysis in specific areas without compromising the overall computational efficiency. Nevertheless, it is imperative to conduct a comprehensive finite element model representation of a more complex model before employing the submodelling technique to ensure its effectiveness and reliability in diverse crash scenarios.

Appendix

By utilizing the graphic approximation technique illustrated in Figure 37, it is possible to obtain the rise time, plateau duration, and acceleration values (g) along the x and y axes at a specific time based on acceleration-time plots derived from measurements or computations [21].

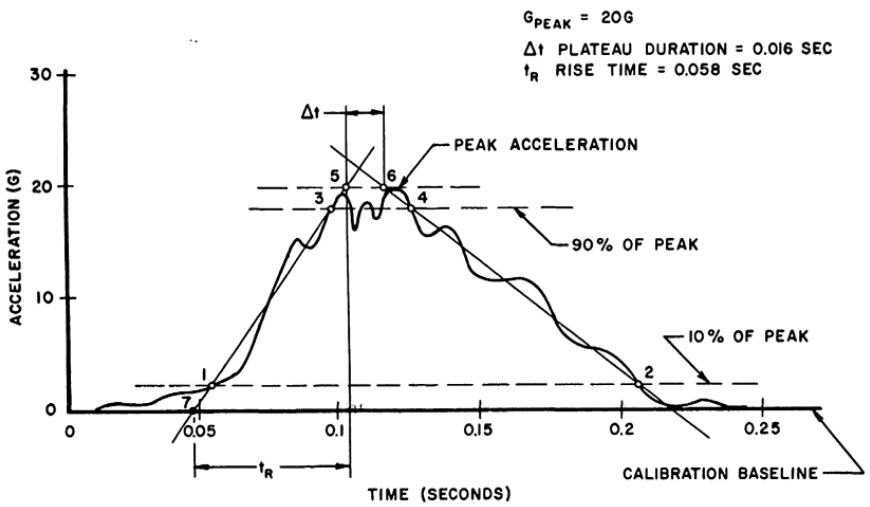

Fig. 37 Graphic Approximation Example [21].

1) Establish the calibration baseline, correcting for any gravity bias acceleration.
2) Establish the maximum (peak) acceleration magnitude.
3) Construct a reference line parallel to the calibration baseline at a magnitude equal to 10 percent of the peak acceleration. The intersection of this line with the acceleration time plot defines points 1 and 2 in Figure 37.
4) Construct a second reference line parallel to the calibration baseline at a magnitude equal to 90 percent of the peak acceleration. The intersection of this line with the acceleration time plot defines points 3 and 4 in Figure 37.
5) Construct the onset line defined by the straight line through points 1 and 3.
6) Construct the offset line defined by the straight line through points 2 and 4.
7) Construct a line parallel to the calibration baseline, through the peak acceleration. The time interval defined by the intersections of this line with the constructed onset and offset lines (points 5 and 6) is the plateau duration

(Δ_t).

8) Locate the intersection of the constructed onset line with the calibration baseline (point 7). The time interval defined by points 7 and 5 is the rise time (T_R).

9) For a given plot of accelerations in the x and y axes, the specific g values are graphically obtained from the constructed onset and offset lines for the specific time at which the summation vector of acceleration is the greatest. An example is shown on Figure 38.

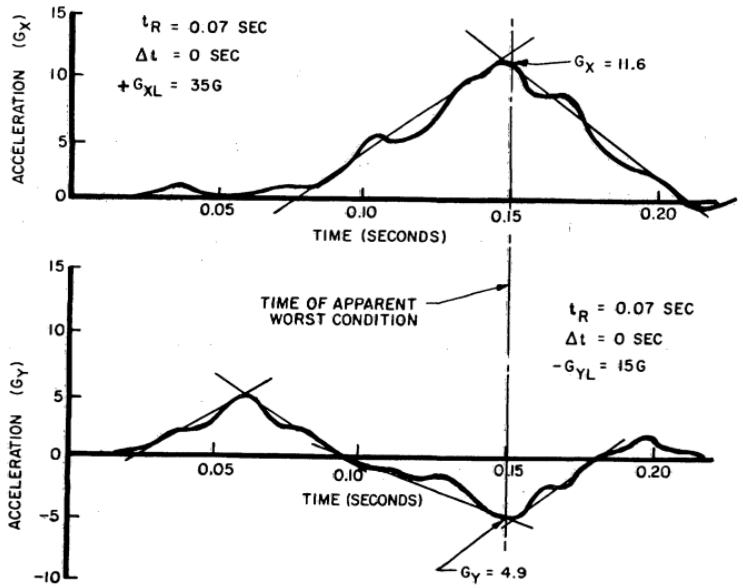

Fig. 38 Multiaxial Acceleration Environment Example [21].

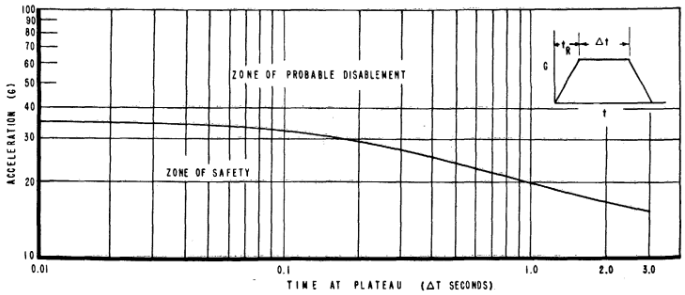

Δt (SEC)	0-.03	.06	.084	.13	.15	.18	.22	.27	.32	.38	.45	.52	.61	.73	.87	1.0	1.22	1.5	1.92	2.45	3.0
G	35	34	33	32	31	30	29	28	27	26	25	24	23	22	21	20	19	18	17	16	15

Fig. 39 Acceleration Limit ($+G_{xL}$) (Rise Time $\geq$ .03 Sec) [21].

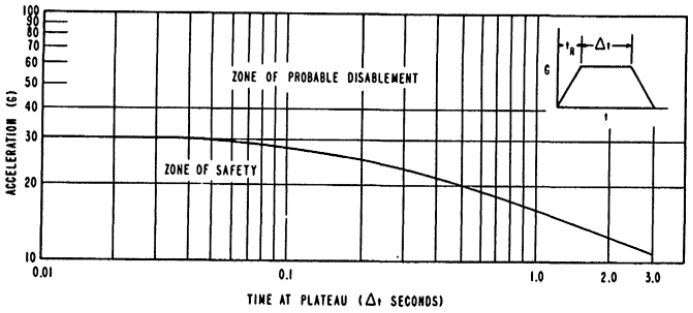

Δt (SEC)	0-.03	.05	.08	.11	.15	.2	.23	.30	.33	.38	.45	.6	.75	.9	1.0	1.2	1.5	1.9	2.5	3.0
G	30	29	28	27	26	25	24	23	22	21	20	19	18	17	16	15	14	13	12	11

Fig. 40 Acceleration Limit ($-G_{xL}$) (Rise Time $\geq$ .03 Sec) [21].

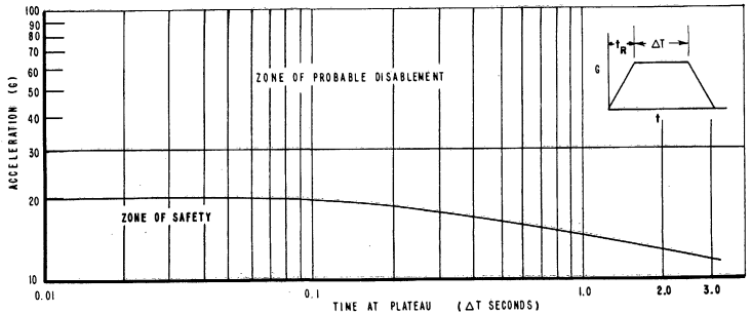

Δt (SEC)	0-.03	.085	.15	.25	.36	.52	.75	1.1	1.6	3.0
G	20	19.5	19	18	17	16	15	14	13	11.5

Fig. 41 Acceleration Limit ($\pm G_{xL}$) (Rise Time $\leq$ .03 Sec) [21].

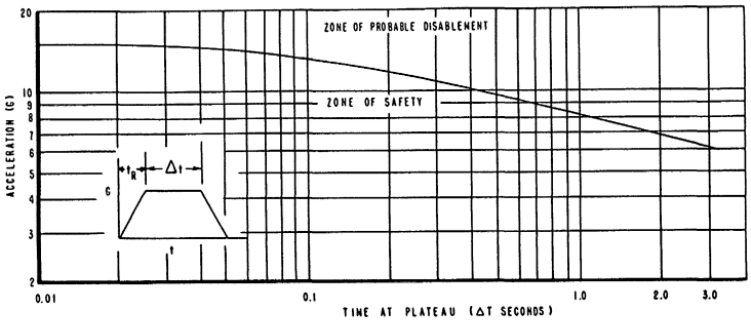

Δt (SEC)	0-.03	.06	.11	.18	.28	.41	.62	.86	1.6	3.0
G	15	14	13	12	11	10	9	8	7	6

Fig. 42 Acceleration Limit ($\pm G_{yL}$) (Any Rise Time) [21].

Acknowledgments

I would like to express my gratitude to Dassault Systèmes for providing the platform and tools essential for developing this thesis, with special thanks to Andrea Villa for his support as my co-supervisor.

References

[1] Dotman, T. P., "A Structural Sizing Methodology for the Wing-Fuselage of the Flying-V," Master's thesis, Aerospace Engineering, 2021. Available at https://repository.tudelft.nl/record/uuid:69e21e65-7168-4f83-abf5-b646bb4c7fe5.

[2] Desiderio, M., "Flying-V Crashworthiness: a Preliminary Assessment," Master's thesis, Aerospace Engineering, 2023. Available at https://repository.tudelft.nl/record/uuid:f9ecffa8-7276-4fab-9f2d-191b92c40e05.

[3] Desiderio, M., Schuurman, M., Alderliesten, R., and Castro, S. G. P., "Crashworthiness of the Flying-V Aircraft Concept with Vertical Drop Test Simulations," *ASIDIC*, 2023. https://doi.org/10.31224/3034.

[4] Oosterom, W., and Vos, R., "Conceptual Design of a Flying-V Aircraft Family," *AIAA AVIATION 2022 Forum*, American Institute of Aeronautics and Astronautics, 2022. https://doi.org/10.2514/6.2022-3200.

[5] Guida, M., Lamanna, G., Marulo, F., and Caputo, F., "Review on the design of an aircraft crashworthy passenger seat," *Progress in Aerospace Sciences*, Vol. 129, 2022, p. 100785. https://doi.org/10.1016/j.paerosci.2021.100785.

[6] Martin, E., "Statistical summary of commercial jet airplane accidents," , 2021. URL https://skybrary.aero/sites/default/files/bookshelf/32664.pdf.

[7] Benad, J., "The technology behind the Flying-V," , Accessed on the 2024/Nov/05. URL https://www.tudelft.nl/en/ae/flying-v/technology.

[8] Liebeck, R., "Design of the blended-wing-body subsonic transport," *40th AIAA Aerospace Sciences Meeting & Exhibit*, 2002. https://doi.org/10.2514/6.2002-2.

[9] Anand, S., Alderliesten, R., and Castro, S. G., "Crashworthiness in preliminary design: Mean crushing force prediction for closed-section thin-walled metallic structures," *International Journal of Impact Engineering*, Vol. 188, 2024, p. 104946. https://doi.org/10.1016/j.ijimpeng.2024.104946.

[10] Anand, S., Alderliesten, R., and Castro, S. G., "Corrigendum to "Crashworthiness in preliminary design: mean crushing force prediction for closed-section thin-walled metallic structures" [International Journal of Impact Engineering, Volume 188, June 2024, 104946]," *International Journal of Impact Engineering*, Vol. 194, 2024, p. 105086. https://doi.org/10.1016/j.ijimpeng.2024.105086.

[11] Administration, F. A., "The Federal Register," , 2022. URL https://www.ecfr.gov/current/title-14/chapter-I/subchapter-C/part-25.

[12] Agency, E. U. A. S., "CS-25 Amendment 27 - review of Aeroplane Performance Requirements for Air Operations and regular update of CS-25," , Jan 2023. URL https://www.easa.europa.eu/en/document-library/certification-specifications/cs-25-amendment-27.

[13] Register, F., "Special Conditions: Boeing Model 787-8 Airplane," , Sep 2007. URL https://www.federalregister.gov/documents/2007/09/26/E7-18942/special-conditions-boeing-model-787-8-airplane-crashworthiness.

[14] SAEJ885, *Human tolerance to impact conditions as related to motor vehicle design (Version 198004)*, Society of Automotive Engineers, Inc., 1980.

[15] Olivares, G., et al., "Anthropomorphic Test Dummy Lumbar Load Variation," *International Technical Conference on the Enhanced Safety of Vehicles*, 2018. URL https://www.researchgate.net/publication/327306747.

[16] Coltman, J. W., Ingen, C. V., Johnson, N. B., and Zimmermann, R. E., *Aircraft crash survival design guide*, Vol. 2, U.S. Army Aviation Research and Technology Activity (AVSCOM), Aviation Applied Technology Directorate, 1989.

[17] Brinkley, J. W., and Shaffer, J. T., *Dynamic simulation techniques for the design of escape systems: Current applications and Future Air Force Requirements*, Aerospace Medical Research Laboratory - Wright-Patterson Air Force Base, 1971.

[18] Stech, E. L., and Payne, P. R., *Dynamic models of the human body*, Aerospace Medical Research Lab, 1969.

[19] Administration, F. A., "Aviation Rulemaking Advisory Committee; Transport Airplane and Engine Issues; New Task," , Jun 2015. URL https://www.federalregister.gov/documents/2015/06/04/2015-13542/aviation-rulemaking-advisory-committee-transport-airplane-and-engine-issues-new-task.

[20] Administration, F. A., "Transport Aircraft Crashworthiness and Ditching Working Group Report to FAA," , Sep 2018. URL https://www.faa.gov/regulations_policies/rulemaking/committees/documents/index.cfm/document/information/documentID/3743.

[21] MIL-S-9479B, U., "Military Specification: Seat System, Upward Ejection, Aircraft, General Specification," *EverySpec*, 1971.

[22] da Costa, T. F., "Crashworthiness Assessment of the Flying-V Under Complex Crash Scenarios with Partially Detailed Structures," Master's thesis, Aerospace Engineering, 2024. Available at https://repository.tudelft.nl/record/uuid:c9bd679a-d43f-4eb2-b282-bcf352510669.

[23] Koenderink, R., "Design Methodology for Unconventional Engine Mounting Structures, Including Crashworthiness Assessment," Master's thesis, Aerospace Engineering, 2024. Available at https://repository.tudelft.nl/record/uuid:2a250390-05c0-4f71-bf73-a21e4cf6567d.